MDPI

*Article*

# Aircraft Emissions, their Plume-Scale Effects, and the Spatio-Temporal Variability of the Atmospheric Response: a Review

**Kieran Tait [1,†,‡], Firstname Lastname [1,‡] and Firstname Lastname [2,*]**

[1] University of Bristol; kt16229@bristol.ac.uk
[2] Affiliation 2; e-mail@e-mail.com
* Correspondence: e-mail@e-mail.com; Tel.: (optional; include country code; if there are multiple corresponding authors, add author initials) +xx-xxxx-xxx-xxxx (F.L.)
† Current address: Affiliation 3
‡ These authors contributed equally to this work.

**Keywords:** keyword 1; keyword 2; keyword 3 (List three to ten pertinent keywords specific to the article; yet reasonably common within the subject discipline.)

**Citation:** Tait, K.; Lastname, F.; Lastname, F. Aircraft Emissions, their Plume-Scale Effects, and the Spatio-Temporal Variability of the Atmospheric Response: a Review. *Aerospace* **2021**, *1*, 0. https://doi.org/

Received:
Accepted:
Published:

**Publisher's Note:** MDPI stays neutral with regard to jurisdictional claims in published maps and institutional affiliations.



## 1. Introduction

Aircraft act as high-altitude emissions vectors, transporting a number of radiatively and chemically active substances across vast regions of the globe. These substances induce a net global warming effect that constitutes 3.5% of global climate change due to anthropogenic emissions [1]. Two thirds of this impact result from the climate forcing of non-CO2 emissions, primarily through emission of nitrogen oxides ($NO_x$), water vapour ($H_2O$) and particulate matter (PM). Emissions of $NO_x$ indirectly affect the climate through photochemical reactions that generate ozone ($O_3$) and deplete methane ($CH_4$), leading to a net warming effect. In sufficiently cold and humid air, water vapour in the aircraft exhaust plume condenses around emitted aerosol particles to form water droplets, which then freeze to form ice crystals in the aircraft wake. The formation of ice crystals in the aircraft wake constitutes what is known as a condensation trail (contrail). Contrails can grow due to uptake of surrounding water vapour and persist for hours, spreading over hundreds of kilometres of the atmosphere, with the possibility of transitioning into cirrus clouds known as contrail cirrus. Persistent contrails and contrail cirrus are known to trap heat more efficiently than they reflect inbound solar radiation, thus exhibiting a net warming effect, thought to be the most significant contribution to aviation-induced climate change [2]. The dependence of these climatic effects on the state of the background atmosphere (i.e. its chemical composition and meteorology) and the time of day and year on which occur, means the climate impact of aviation is spatio-temporally sensitive, with the same emissions released at different times and/or locations potentially leading to very different climate effects. This means that flying around particularly climate-sensitive regions of the atmosphere has the potential to reduce aviation's climate impact, with simulations from Niklaß et al. (2019) [**?** ] showing a 12% reduction at virtually no additional cost of fuel burn.

The dispersion of aircraft emissions occurs over great length and time scales, with emissions entrained in the aircraft exhaust plume which spreads hundreds of kilometres [3] over its lifetime of up to 12 hours [4]. The elevated concentrations of emissions species present within the plume result in additional nonlinear chemical (gas-phase and heterogeneous) and microphysical processes which are not accounted for in global chemistry models, due to the inherent assumption of instantaneous dispersion (ID) of emissions. The ID assumption models emissions as homogeneously mixed into the volume of the computational grid cell in which they are released into, thus neglecting any

subgrid-scale nonlinear processing that may occur throughout the plume lifetime [5]. The inclusion of plume-scale modelling in the analysis of aviation climate impact captures the initial depletion of ozone in the plume due to the saturation of $NO_x$ emissions, followed by the conversion of $NO_x$ to nitrogen reservoir species (e.g. $HNO_3$) on the order of 10%, which are less efficient at producing ozone when propagated to global scales. The lack of accounting of these in-plume processes in the ID approach results in an overestimation of ozone forming potential by up to ~20% [6]. Furthermore, heterogeneous reactions that take place on aviation-induced aerosol particles in the plume can lead to the self reaction of a key oxidant known as the hydroperoxy radical ($HO_2$), thus leading to further reduction of ozone production that is overlooked in global modelling efforts []. Insufficient microphysical modelling of contrails in aircraft exhaust plumes has also been shown to limit accuracy of climate impact calculations in global models []. The formation and persistence of contrails can be deduced purely from the satisfaction of thermodynamic criteria related to the saturation of ice and water in the surrounding atmosphere. However, determination of the evolution and radiative impact of contrails requires the microphysical analysis of key optical and physical properties, meaning the improper accounting of contrail and aerosol microphysics in global models leads to large uncertainties in the true global atmospheric impact of contrails [].

The ideal solution to the issue of inadequate accounting of subgrid-scale effects in global models would be to obtain high-resolution plume model data for every flight that takes place. In reality, flights take place in the hundreds of thousands every day, so the computational load from such a task would be exceedingly large []. Instead, plume models and large eddy simulations are used to deduce and calibrate parametrisations of these plume-scale processes, that can be applied to global models to capture the subgrid-scale effects without the need for full plume model implementation. Parametrisations of gas-phase conversions in the plume have been covered extensively in the literature, however the global modelling of heterogeneous chemistry and contrail microphysics is an area that is more difficult to approach, and work is still ongoing to reduce uncertainty in this area [].

The degree to which nonlinear chemical and microphysical processing occurs in aircraft plumes varies with respect to temperature, time of emission, latitude, season, turbulence, and the background concentrations of key chemical species, primarily $NO_x$ and $O_3$ [**?** ]. This means that discrepancies between plume models and global models also deviate with location and time, and any attempts to parametrise plume processes into global models must take this spatio-temporal variability into account. The sensitivity of plume processes to environmental conditions also transfers to scenarios where multiple plumes overlap in high density airspace. The accumulation of emissions due to overlapping plumes in high-density airspace can lead to exceptionally high concentrations of key chemical species, with $NO_x$ and cloud condensation nuclei (CCN), such as soot and sulphate aerosol particles, expected to increase the most [7,8]. The perturbation to the chemical state of the atmosphere due to other aircraft emissions has been shown to have a considerable effect on the eventual climate impact of further emissions released, with the saturation of $NO_x$ leading to further reductions in ozone formation [] and the dehydration of water vapour due to prior contrails leading to a diminishing effect of subsequent contrails released into the same volume of airspace []. Quantifying aviation's atmospheric impact on subgrid-scales therefore requires determination of the atmospheric state, and the integration of air traffic data, to deduce the perturbation of the atmospheric state due to prior flights through the same region of airspace.

This review article documents the current state of literature on aviation's atmospheric effects and the influence of nonlinear plume-scale processing on the global net climate impact. Section 2 covers the emissions generation process and the methods used to model aircraft performance and emissions. Section 3 explores the dispersion characteristics of aircraft emissions on the subgrid scale, alluding to the various modelling methods developed to investigate the dynamical characteristics of aircraft plumes.

In section 4, air traffic management principles and their effect on aviation emissions distribution is considered, on both the local and global scale, followed by section 5 which explores aircraft climate impact, based on the emissions released and the chemical and physical processes that occur on the grid and subgrid-scale of global models. Section 6 looks into the effect of subgrid-scale processes that occur due to emissions accumulation in high-density airspace, and finally section 7 explores potential mitigation efforts to reduce aviation-induced climate change through changes to aircraft operations, such as climate-optimal routing and formation flight.

## 2. Aircraft emissions

Aircraft propulsion systems provide the essential driving force component to enable powerful and efficient flight. Throughout history, convention has dictated the use of hydrocarbons as the primary fuel source for aircraft propulsion since the dawn of powered flight, due to their unparalleled energy content and ease of availability. In modern commercial aviation, responsible for ~88% of global aviation fuel usage [9], it is commonplace to use a gas turbine propulsion system operating on kerosene-based jet fuel. Aviation's environmental impact stems from the emission and dispersion of chemically and radiatively active substances, that are generated during the jet fuel combustion process. The combustion of fuel and the generation of emissions is closely coupled with the performance of aircraft, and the forces experienced throughout flight. This section explores the coupling between aircraft performance and the generation of aviation-induced climate forcing species, before reviewing the emissions modelling techniques present in the current literature.

### *2.1. The need for propulsion*

For an aircraft to achieve and maintain airborne status, it is required that the resistive force due to aerodynamic drag (D) and the gravitational force due to aircraft weight (W) are sufficiently overcome. The necessary driving force required to counteract drag and maintain forward speed is known as thrust (T). The forward speed induces airflow over the aircraft's cambered wings, thus rotating the flow downwards and generating lift (L) to counteract the aircraft weight. These constitute the four fundamental forces of flight [10]. The combination of these forces in varying magnitudes determines the trajectory of an aircraft and its instantaneous velocity and acceleration. The performance of an aircraft is highly dependent on the optimisation of the four forces, with structural configuration, material utilisation and payload affecting the aircraft's weight, balance and stability, and the aircraft geometry affecting aerodynamics and hence influencing the lift and drag forces acting upon it. The thrust force however, is generated by means of a propulsion system.

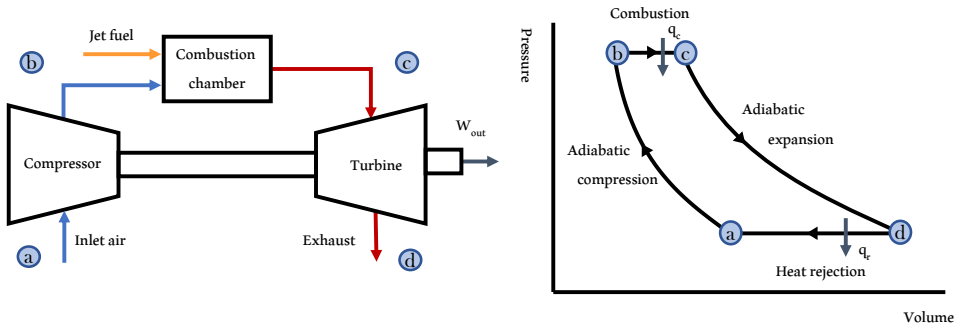


**Figure 1.** The open-cycle Brayton thermodynamic cycle and its corresponding pressure-volume diagram, adapted from [].

Traditional gas turbine engines, known as turbojet engines, employ the following four point Brayton thermodynamic cycle (see figure 1): (a–b) the engine ingests oncoming

air flow and passes it through a compressor, reducing volume and increasing total pressure; (b–c) the compressed air is mixed with fuel and ignited to cause a combustion reaction, with $q_c$ representing the heat addition to the system; (c–d) the high temperature, high pressure combustion products are passed through a turbine which extracts some energy from the flow to do work ($W_{out}$) to drive the compressor; (d–a) the airflow leaves the engine and is rejected into the atmosphere ($q_r$) at an accelerated rate through the exhaust nozzle. The magnitude of thrust generated by the engine is dependent on the mass of air being accelerated, and the difference in velocity of the air mass through the propulsion system [11]. The commercial fleet of today primarily use bypass turbofan engines, which have an additional fan installed at the engine inlet. This fan is also powered by the turbine and its purpose is to bypass most of the intake air through the outer duct (often around ~90% according to modern day bypass ratios []. The addition of a bypass fan serves to increase the mass flow of air being accelerated by the engine, generating additional thrust without the need to burn additional fuel. This leads to a net increase in fuel efficiency of the engine compared to the turbojet equivalent, as the additional thrust generated due to the bypass design outweighs the additional fuel burn required to power the fan [12].

### *2.2. The jet fuel combustion process*

The widespread usage of kerosene-based jet fuels stems from the need to satisfy strict power-to-weight and safety requirements demanded by commercial aircraft; this is because kerosene has an exceptionally high energy density and wide operating temperature range at a low financial cost, compared with alternative fuel types [13**?** ]. The stoichiometric combustion of kerosene with air required to generate thrust, does however generate a number of chemically and radiatively active emission species which are emitted from the aircraft into its wake. These aircraft emissions interact with the surrounding atmosphere, perturbing the natural balance of chemistry and contributing to air quality issues and anthropogenic climate change. The mass of emission produced per unit mass of fuel burnt is often referred to as the emission index (EI), measured in grams of emission per kilogram of fuel [g/kg].

The primary products of ideal jet fuel combustion are carbon dioxide ($CO_2$), water vapour ($H_2O$) and, due to fuel impurities, a relatively small amount of sulphur oxides ($SO_x$). These products depend purely on the carbon-hydrogen-sulphur composition of the fuel, meaning they have a constant EI throughout all phases of flight. This means that for a constant fuel composition, these species have a constant EI throughout the entire range of operating conditions and therefore they are directly coupled to the amount of fuel burnt [14]. Further to this, a number of secondary combustion products are generated in the aircraft exhaust, namely oxides of nitrogen ($NO_x$ = NO + $NO_2$), carbon monoxide (CO), unburnt hydrocarbons (HC), particulate matter (PM) and trace levels of volatile organic compounds (VOCs) [7]. These products differ in that their EIs are variable depending on aircraft engine type, engine operating conditions, and the atmospheric conditions of the surrounding environment [15].

### *2.3. The generation of aircraft emissions*

$NO_x$ emissions originate from the entry of atmospheric nitrogen ($N_2$) into the high temperature combustion chamber. The level of $NO_x$ increases with increasing temperature and pressure, as it is coupled to the thermal reaction processes that occur in the primary combustion zone. Therefore, with the assumption of constant polytropic and combustion efficiencies, the emission index of $NO_x$ ($EINO_x$) can be correlated with aircraft fuel flow [16,17]. As a result of inefficiencies in the combustion process, products such as CO and HC are formed. Contrarily to $NO_x$, these emissions are direct products of incomplete combustion, meaning their concentrations are inversely proportional to combustion efficiency. Since combustion efficiency correlates with thrust for sea level

static (SLS) conditions, and thrust correlates with fuel flow, this means that EICO and EIHC decrease with increasing fuel flow.

PM emissions from aircraft can be categorised by their volatility: non-volatile PM (nvPM) and volatile PM (vPM). The primary source of nvPM present in aircraft exhaust is soot, which constitutes the greatest warming effect of all particles released from aircraft [18]. Soot is generated in the fuel rich regions of the combustor, where the condensation of unburnt aromatic hydrocarbons takes place, converting low carbon content HC fuel molecules into carbonaceous agglomerates containing millions of carbon atoms [19,20]. The extent of soot formation therefore depends on the fuel-air-ratio and the mixing processes that take place in the combustor, which vary with combustor design and are influenced by the non-homogeneous flow and temperature fields. Accurate measurements of these parameters are rare, making it very difficult to directly acquire quantitative data on soot emissions. Instead, soot EI can be estimated based on correlation with the so-called smoke number measured in engine certification procedures [16].

The formation of vPM from aircraft largely derives from the emission of sulphur derivatives, lubrication oil and VOCs [21]. During combustion, the sulphur content in the fuel is mostly oxidised to sulphur dioxide ($SO_2$), some of which is then further oxidised to sulphuric acid ($H_2SO_4$) when emitted into the atmosphere. In the presence of sufficient water vapour, sulphate aerosols ($SO_4$) can be generated, which exhibit the largest cooling effect from aircraft PM emissions [14]. The sulphate EI is a factor of fuel sulphur content, which varies depending on fuel composition and the specific emissions characteristics of the engine [22]. Due to the low volatility of lubricant oil, the emitted oil vapour from aircraft will add to the condensed mass of VOCs and contribute to vPM concentrations. The VOCs produced either from the oxidized fuel fragments or due to the pyrolysis in the combustion chamber can also act as vPM, which may have sufficiently low vapour pressure to allow condensation in the atmosphere forming a coating on the surface of the nvPM, impacting cloud formation, precipitation and climate [14]. The particulate matter emitted near the exit nozzle plane of the combustor consists only of nvPM. However vPM are produced through nucleation and condensation downstream. Thus it is difficult to estimate the total amount of vPM produced within the exhaust plume, as the formation of vPM is dependent on the concentration of sulphates and VOCs present in the exhaust, and the distance from the combustor [].

### *2.4. Aircraft emissions modelling*

Accurate quantification of aircraft emissions for any given flight requires the calculation of aircraft performance to estimate the total energy consumed, and hence, the total fuel burnt throughout the flight duration. With knowledge of fuel flow rates experienced throughout flight, flow rates of aircraft emission species can be deduced based on empirical engine performance datasets and emissions models.

#### 2.4.1. Fuel burn estimation

Computational modelling of aircraft performance allows the simulation of aircraft trajectories and the quantification of forces experienced throughout flight, enabling the approximation of thrust and fuel flow across all phases of flight. Aircraft performance models that are prevalent in academia and industry, such as the BADA (Base of Aircraft DAta) method [23] and Piano-X [24], emulate aircraft behaviour by coupling a database of aircraft-specific performance datasets to mathematical models to calculate useful flight characteristics, such as fuel flow and fuel burn, at discrete time steps during flight. This iterative approach accounts for the time-varying nature of aircraft properties like mass, speed and heading, thus leading to a more accurate estimate of performance and fuel burn estimation. Further to this, models such as the Aviation Environment Design Tool (AEDT) [25] exist, which carry out four-dimensional (4-D) physics-based simulations of aircraft trajectories at an exceptionally high spatial and temporal resolution, providing highly accurate predictions of fuel consumption and localised emissions impacts. Such

tools do however come at the expense of high computational and financial cost, and often require proprietary data that is unavailable to the public domain. An alternative state-of-the-art open-source performance model that has been made available in recent years is the OpenAP model [26]. This model consists of four main components; the aircraft and engine property model, the kinematic and dynamic aircraft performance models, and utility libraries; and can describe the characteristics of 27 common aircraft and 400 turbofan engines, deeming it a feasible alternative for researchers who do not have access to proprietary data and licensing for the other more established models.

#### 2.4.2. Calculating aircraft emissions at reference conditions

Aircraft performance models provide estimates of aviation fuel burn, but to estimate the particular chemical speciation of emissions released due to fuel combustion, aircraft emissions models must be implemented. As alluded to previously, the primary combustion products, $CO_2$, $H_2O$ and $SO_2$, have a direct relation to the amount of fuel burnt and hence a constant EI for a given fuel composition, with standard estimates provided in table **??**. Secondary combustion products such as $NO_x$, CO and HC however, largely depend on operational and atmospheric conditions. Empirical relationships between EI and fuel flow for secondary combustion products have been determined at reference operating conditions using engine performance datasets, such as the International Civil Aviation Organisation (ICAO) engine emissions databank [27]. This databank was developed for the purpose of engine certification and compliance with landing and take-off (LTO) cycle emissions standards, outlined in ICAO Annex 16 Vol. II [28]. Engine test data have been collected at sea-level static (SLS), International Standard Atmosphere (ISA) conditions, for four reference operating conditions (thrust settings) relevant to the LTO cycle: take-off (100% thrust), climb out (85%), approach (30%) and taxi in/out (7%). For every engine at each of the four LTO modes, a reference fuel flow and corresponding emission index has been derived, allowing emissions to be estimated for aircraft operating under any of the four modes, to a reasonable degree of accuracy. An exemplary ICAO EI dataset is provided in table **??**.

**Table 1:** Emission indices estimates for $CO_2$, $H_2O$ and $SO_2$, averaged from a range of existing studies testing various aviation fuel types [**?** ].

| $CO_2$ | $H_2O$ | $SO_2$ |
|---|---|---|
| 3.149 g/kg fuel | 1.230 g/kg fuel | 0.84 g/kg fuel |

**Table 2:** Example ICAO engine emissions data for Rolls Royce Trent 970-84 engine [27].

| | **Take-off** | **Climb out** | **Approach** | **Idle** |
|---|---|---|---|---|
| **Fuel flow [kg/s]** | 2.605 | 2.157 | 0.720 | 0.255 |
| **EI $NO_x$ [g/kg]** | 38.29 | 29.42 | 12.09 | 5.44 |
| **EI CO [g/kg]** | 0.32 | 0.31 | 1.16 | 13.38 |
| **EI HC [g/kg]** | 0.02 | 0.12 | 0.08 | 0.04 |

#### 2.4.3. Calculating aircraft emissions at non-reference conditions

In reality, aircraft spend the majority of flight outside of the LTO vicinity (above 3,000 ft), and the operating conditions and atmospheric conditions vary considerably. To enable the accurate analysis of aircraft emissions outside of reference conditions, a number of emissions modelling methods have been developed. Such methods apply the necessary adjustments and interpolations to the LTO-limited engine performance datasets, to generate more realistic estimates of aircraft emissions across the whole flight profile. SAE International Aerospace Information Report 5715 (AIR5715) [29] describes a number of methods for calculating aircraft emissions throughout all modes

of operation and compares their relative merits. For the primary combustion species, the Fuel Composition method is presented, which determines $EICO_2$, $EIH_2O$ and $EISO_x$ from the proportions of carbon, hydrogen and sulphur in the fuel. The set of methods concerning the estimation of $EINO_x$, EICO and EIHC include the ICAO reference method, the Boeing fuel flow method 2 (BFFM2), the DLR fuel flow method and the P3T3 method, in order of increasing fidelity. The ICAO reference method serves as the simplest and least accurate approach, computing emissions purely based on the ICAO reference conditions, without applying corrections to account for atmospheric effects at altitude. Therefore, it is only applicable for emissions analysis of aircraft flying in the LTO region. The remaining methods, BFFM2, DLR and P3T3 can be applied at all aircraft operating conditions, including at cruise, as they apply interpolations to engine performance datasets to determine emissions indices throughout the whole duration of a flight. The BFFM2 method and the DLR method ($NO_x$ only) are the mid-tier models, as they provide reasonable estimates of EIs purely from interpolating the EI reference data and applying corrections for atmospheric effects based on ambient meteorological data, aircraft fuel flow and Mach number. The gold standard for modelling of $NO_x$, CO and HC emissions is however, the P3T3 method, as it utilises detailed thermodynamic modelling data to determine the precise emission indices at any given point throughout flight. Required data includes the combustor inlet temperature (T3), pressure (P3) and the fuel-air ratio (FAR) at both reference and operational conditions. All of which are difficult to obtain without access to proprietary engine-specific performance data, which limits the accessibility of this model to open-access researchers [**?** ].

See figure 2 for an example of how EIs are interpolated based on the logarithmic relationship between EI and fuel flow, using the BFFM2 method [30]. Furthermore, methods are also presented to account for the remaining key emission species, such as the Derivative Factor method [25] used to approximate the EI values for VOCs such as non-methane HC (NMHC) throughout flight and the First Order Approximation method [21] used to estimate PM emission indices. The choice of method generally depends on the emission species to be observed, the compromise between modelling resources and data availability, and the level of accuracy required.

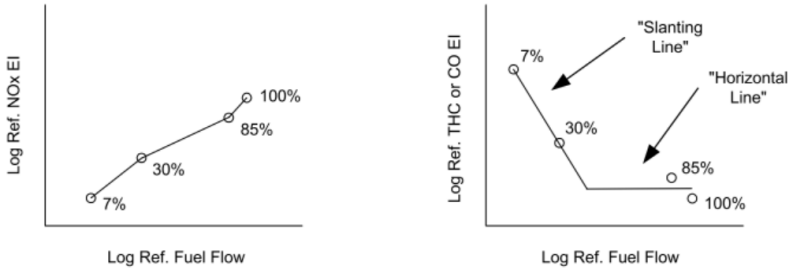


**Figure 2.** Example log-log plots of EI against fuel flow at reference conditions, as prescribed by the BFFM2. The percentage values refer to the thrust as a percentage of maximum thrust at SLS conditions [29].

#### 2.4.4. Emissions inventories and integration into large-scale climate models

The estimation of aircraft emissions for a specific flight involves the simulation of aircraft performance across the entire flight profile so as to estimate fuel flow and engine operating conditions throughout flight. Knowledge of fuel flows and engine performance characteristics permits the estimation of aircraft emissions, based on the coupling of empirical engine certification data and emissions modelling methods, which interpolate the data to determine the emissions at non-reference conditions. This emissions estimation procedure is commonly carried out on a regional and global scale to determine emissions from a whole range of flights, which are then stored in so-called emissions inventories [31]. Aircraft emissions inventories collate data from all flights in

the desired range and populate three-dimensional (3-D) latitude-longitude-altitude grid cells (e.g. 1°× 1°× 1000 ft) with total emissions quantities [5].

Aircraft emissions inventories are utilised to model the atmospheric effects of aviation, using a large-scale chemical transport model (CTM) or a climate-chemistry model (CCM), which captures the chemistry, physics and dynamics of the Earth-atmosphere system. Such models allow one to simulate the perturbation to the state of the atmosphere due to an input of emissions and, in turn, provide quantitative indicators that enable modellers to determine the resultant climate impact (e.g. concentrations of key greenhouse gases, aerosol formation and distribution, cloud processes etc.) [32]. However, one underlying issue with this conventional approach to aviation climate modelling, is that the use of gridded emissions data inherently assumes the instantaneous dispersion (ID) of emissions into the atmosphere [33]. The ID approach assumes that aircraft emissions are instantaneously dispersed into the latitude-longitude-altitude computational grid cell in which they were released. The dimensions of this grid cell are solely determined by the spatial resolution of the global model, and hence do not serve as an accurate physical representation of emissions dispersion.

In reality, emissions released from aircraft are confined to the aircraft exhaust plume, which inhibits mixing with the surrounding atmosphere for up to a day after emission. Throughout this time, a number of nonlinear chemical and microphysical processes occur, due to the elevated concentrations of emissions species in the plume. These nonlinear plume-scale processes affect the eventual climate response to these emissions, yet most regional and global aviation climate impact studies [34] often neglect the presence of the aircraft exhaust plume and opt for the simplified ID method. The following section explores the dynamical evolution of emissions following their release into ambient air, and discusses modelling approaches present in the literature which can be implemented to represent plume-scale effects in large-scale models. Such modelling is, however, often set aside due to computational issues associated with resolving consistency between the two model resolutions.

## 3. The dispersion of aircraft emissions and the aircraft exhaust plume

Following their expulsion into the free atmosphere throughout flight, aircraft exhaust gases are confined to a plume that undergoes a series of dynamical regimes (**jet**, **vortex**, **dispersion** and **diffusion** regimes), before becoming fully diluted in the surrounding air. The entrainment of emissions within the plume throughout these dynamical regimes leads to initial species concentrations that are several orders of magnitude higher than background levels [35], giving rise to a number of nonlinear chemical and microphysical effects. These plume-scale effects have considerable implications on the eventual chemical composition of the surrounding atmosphere and lead to the formation of aerosols and ice crystals in the aircraft wake. Therefore, inclusion of plume-scale effects is vital for high fidelity modelling of aviation's impact on the climate.

### *3.1. Plume-scale dynamical regimes*

In order to accurately account for nonlinear effects experienced in the aircraft exhaust plume, one must first understand the dynamical response of the plume after combustion, to gauge the length and time scales over which aircraft emissions are entrained within it.

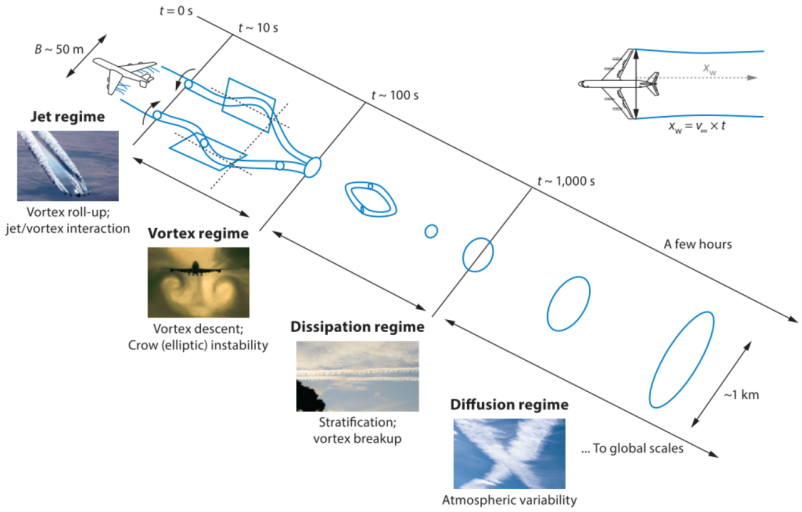


**Figure 3.** Aircraft exhaust plume dynamical regimes. Wake distance behind aircraft $x_w = v_\infty \times t$ where $v_\infty$ is aircraft speed and $t$ is the post emission time [36,37].

Exhaust gas temperatures range from around 1500 K post combustion, 600 K at engine tailpipe, followed by mixing with bypass air cooling the flow to around 300 K [7] as the dispersion process begins. During the first 1–20 s post emission, an axisymmetric jet is formed, which rapidly diffuses into ambient air and cools to ambient temperatures. Over this period, known as the **jet** regime, the airflow passing over the wings is diverted downwards to generate lift, thus creating a vortex sheet at the trailing edge of the aircraft. This vortex sheet rolls up into a pair of counter-rotating vortices which are shed at the wing tips. The evolving vortex pair then merge together and propagate downwards, due to their mutually induced downwash velocity, trapping the exhaust plume within their cores and signalling the beginning of the vortex regime.

Throughout the **vortex** regime, which occurs between 20 s and 2 minutes after combustion, the primary wake containing the vortices and trapped exhaust plume sinks by around 150–200 m, resulting in a slight temperature increase of 1–3 K, due to the adiabatic heating of exhaust constituents in the sinking vortices. Further to this, the organised vortical structure means the wake does not grow significantly during this time, and hence the concentrations of entrained chemical species remain relatively constant. The adiabatic heating of the exhaust does however lead to baroclinicity at the border between each vortex and the ambient air, which detrains some momentum, heat and exhaust constituents from the primary wake, to form a secondary wake. This secondary wake trails upwards as it is warmer than the surrounding ambient air, and it escapes the influence of the vortex structure, resulting in enhanced mixing with ambient air and thus experiences different chemical and microphysical processes compared with the primary wake [37].

Following this is the **dispersion** regime, in which the aircraft-induced dynamics subside due to the growth of Crow instability [38], which dissipates and disintegrates the primary and secondary wake vortices [36]. The breakdown of the organised vorticial structure and the production of turbulent motion leads to a sudden increase in the rate of entrainment between the exhaust plume and the ambient air by a factor of 10 [], therefore giving rise to a continuous decay of concentration and temperature within the plume. This regime lasts for 2–5 minutes after combustion, however this varies as the strength of aircraft induced vortices is proportional to the weight and span, and inversely proportional to the speed of the aircraft [37]

Lastly, the plume undergoes its final dynamical event, known as the **diffusion** regime. This regime is characterised by the aircraft-induced dynamics becoming negligible (after about 6 minutes [39]), followed by the subsequent dominance of atmo-

spheric processes in the spreading of the aircraft exhaust plume and its constituents. Atmospheric turbulence, radiation transport and stratification are examples of natural phenomena that contribute to the diffusion of the plume, with total dilution to ambient concentrations often occurring over timescales of 2–12 h post emission [4]. During this time, the plume may spread up to a few kilometres through atmospheric turbulence and shear in the ambient air, diluting the exhaust species over vast volumes of airspace [40].

Plume-scale climate effects that result from the confinement of emissions to the aircraft exhaust plume during the four dynamical regimes considerably alter the eventual global warming effect of a particular flight, and therefore should be appropriately accounted for in modelling efforts to estimate aviation's climate impact.

### *3.2. Plume-scale modelling*

To tackle the issue of neglected plume-scale effects in the computational analysis of aviation-induced climate change, a number of plume modelling methods of varying fidelity have been theorised in the literature. Sub-grid resolution plume models simulate the dynamical response of the aircraft plume, so as to capture the nonlinear chemistry and microphysical effects that occur within it. The outputs of plume models can then be parametrised into low-resolution global models, to increase the accuracy of climate impact calculations through better accounting of the emissions dispersion process.

#### 3.2.1. Empirical dilution model

Plume dynamics control the rate at which aircraft emissions mix and dilute into the surrounding atmosphere, directly affecting the resulting climate impact of aircraft emissions due to the nonlinear effects experienced in the plume, before it becomes homogeneously mixed into the ambient air. Quantifying the rate of dilution and modelling the climate effects that occur within aircraft plumes is therefore an essential process in the accurate analysis of aviation's climate impact [40]. In Schumann et al. (1998) [41], an empirical dilution model was developed to investigate the mixing rate of plumes throughout their typical lifetimes, based on data collated from over 70 aircraft exhaust plume encounters with research aircraft. The characteristic property observed in this study is the plume dilution ratio, $N$, which is defined as the amount of air mass that the exhaust plume generated from a unit mass of fuel burn, mixes with, per unit flight distance within the bulk of the plume.

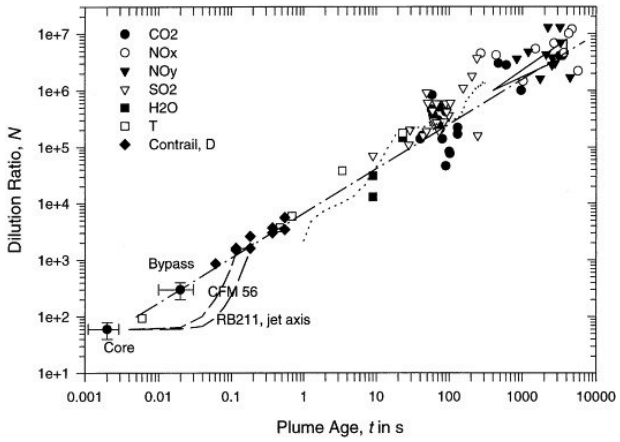


**Figure 4.** Dilution ratio against plume age derived from empirical data. Marker shapes correspond to tracer species as displayed in legend. Markers with error bars correspond to characteristic values for the engine core (leftmost and lower) and bypass exits (rightmost and upper). The dashed curves near the core represent dilution on the jet axis, calculated for two engine types: CFM56 and RB211. The dotted curve represents large eddy simulation results from Gerz and Ehret (1997) []. The range of dilution values computed for large plumes ages by Dürbeck and Gerz (1996) [] are bounded by the triangle, top right of the figure. The dash-dotted line shows the interpolation that is represented by equation (1) [41].

In figure 4, measured dilution ratios from the plume encounters are plotted against plume age. The data was generated by measuring the concentrations of a range of chemical sources across a variety of aircraft types, within the time interval of 0.001 to 10,000s. The significance of these findings is that, in spite of the diverse range of chemical species and aircraft types observed, throughout all four dynamical regimes, a relatively consistent logarithmic relationship emerges between dilution ratio and increasing plume age. When interpolating the regression line fitted to the data in figure 4, the following equation can be obtained where $N$ represents dilution ratio, $t$ is plume age in seconds, and $t_0$ serves as an arbitrary reference scale.

$$N = 7000(t/t_0)^{0.8},\ t_0 = 1s \tag{1}$$

It is evident from the figure however, that encounters with plumes older than 50–100 s tend to diverge from the line fit, indicating a reduction in accuracy of the logarithmic approximation over time. This is likely due to the transition from the organised vortex structure present in the vortex regime, to the turbulent dispersion regime, where more unpredictable atmospheric processes begin to take place and become the primary influence on the evolution of the plume. Therefore, this empirical model can only be used reliably up to the vortex regime. Beyond this, a Gaussian approximation to the distribution of species concentrations is typically employed, accounting for dispersion effects experienced at cruising altitudes, such as advection, gravitational sedimentation, anisotropic diffusion, wind shear and stable stratification [42]. Two popular modelling methods which implement Gaussian approximation and the two-dimensional diffusion equation to model aircraft plumes over their whole lifetime are the Single Plume model and its discretised counterpart, the Multi-layered Plume model.

### 3.2.2. Single and Multi-layered Plume models

The Single Plume (SP) model, first presented in Petry et al. (1998) [33], approximates the time-evolving concentration field of an aircraft exhaust plume using a Gaussian distribution [43]. Petry represents diffusion through eq. (2), a differential equation that describes the temporal variation of exhaust concentration $C$ of species $i$ in the plume

$$\frac{\partial C_i}{\partial t} = -sz\frac{\partial}{\partial y}C_i + D_v\frac{\partial^2}{\partial^2 z}C_i + D_h\frac{\partial^2}{\partial^2 y}C_i + 2D_s\frac{\partial^2}{\partial y \partial z}C_i \tag{2}$$

This two-dimensional diffusion equation is a function of wind shear ($s$), horizontal ($y$) and vertical distance from plume centre ($z$), and the horizontal ($D_h$), vertical ($D_v$) and shear ($D_s$) diffusion coefficients, as calculated based on empirical data recorded under typical atmospheric conditions at aircraft cruising altitudes and assuming a horizontal flight path [44]. The solution to the diffusion equation is a time-varying Gaussian function, with standard deviations $\sigma_h$, $\sigma_v$ and $\sigma_s$ that depend on $s$, $D_h$, $D_v$, $D_s$, time $t$ and the respective initial values ${\sigma_{0h,v}}^2$

$${\sigma_h}^2(t) = \frac{2}{3}s^2 D_v t^3 + (2D_s + s{\sigma_{0v}}^2)st^2 + 2D_h t + {\sigma_{0h}}^2, \tag{3}$$

$${\sigma_v}^2(t) = 2D_v t + {\sigma_{0v}}^2, \tag{4}$$

$${\sigma_s}^2(t) = sD_v t^2 + (2D_s + s{\sigma_{0v}}^2)t. \tag{5}$$

The standard deviations of the Gaussian function can then be used to deduce useful parameters such as plume cross-sectional areas and concentrations. Outputs such as these can serve as input to atmospheric models, enabling the simulation of the dynamical evolution of the plume, and its entrained emissions throughout its lifetime.

The main drawback of the SP model however, is the assumption of homogeneous concentration distribution throughout the plume at any given time. This homogeneity assumption is sufficiently accurate up to the vortex regime, where plume cross-sectional areas are relatively small, entrainment rates are low, and the mixing ratio is relatively consistent across the plume diameter [6]. However, beyond this, the spike in entrainment rates following the breakdown of vortices causes rapid plume expansion, and the drop in concentration from plume core to outer edges becomes increasingly significant [45,46]. This spatial concentration gradient along the plume cross-section cannot be captured using the SP approach, so an alternative model is proposed, known as the Multi-layered Plume (MP) model, as seen in figure 5. The MP model builds upon the SP model by discretising the plume cross-section into a number of concentric rings, enabling the inhomogeneous concentration profile to be represented by varying the mean concentration in each ring.

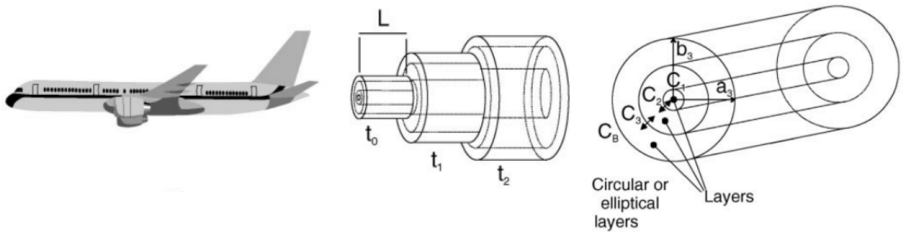


**Figure 5.** MP model visual representation [3]. Plume length L was set to the distance travelled over 1 s (247 m in this scenario) with three out of eight concentric rings shown for each timestep. $C_1 - C_3$ indicate the concentrations in each ring and the arrows represent mixing between the layers.

As Kraabol et al. (2000) [3] states, the Gaussian approximation to emissions dispersion only applies to the dynamical evolution of passive species, and is not suitable for modelling the evolution of chemically active species, due to the nonlinear chemical response in the plume. To counteract this issue, this paper implements an adapted version of the MP model, in which the plume is divided into 8 concentric rings, each with a chemistry module incorporated to estimate the chemical production and loss mechanisms of all species present. Applying this model under assumed turbulent conditions

derived from Dürbeck and Gerz (1996) [47], graphs of horizontal and vertical plume radius are plotted against plume age, as shown in figures 6a and 6b. After just 1 hour, it is predicted that plumes can spread between 1 and 10 km horizontally, whilst only reaching around 50–100 m vertically due to atmospheric stratification [44]. As the plume approaches the end of its typical lifetime, between 10 and 15 h, plume cross-sections can reach 100–200 km horizontally and 200–400 m vertically. The vast length scales over which plumes span throughout their lifetime provides ample evidence to suggest that, in high-density airspace, plumes can overlap. The overlapping of plumes can thus lead to spikes in emissions concentrations that exceed that of single aircraft plumes, thus augmenting nonlinearities in the climate response and further propagating discrepancies between plume and global model outputs [8].

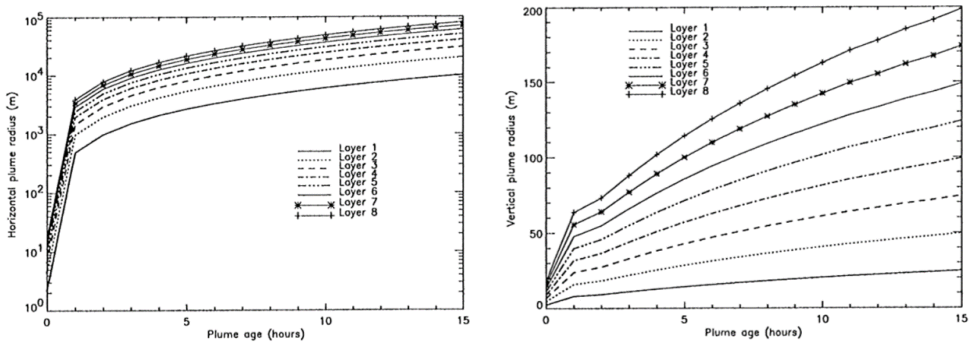


**(a)** Growth in horizontal plume radius over time.**(b)** Growth in vertical plume radius over time.
**Figure 6.** Evolution of plume radius for MP model under assumed turbulent conditions [3].

### 3.2.3. Aircraft Plume Chemistry, Emissions, and Microphysics Model (APCEMM)

Models such as APCEMM from Fritz (2017) [**?** ] further increase the accuracy of the SP and MP models by capturing additional effects that affect plume evolution and hence the resultant climate response once the plume is fully diluted. This includes effects such as plume anisotropy and asymmetry which impact the eventual spatial distribution of the plume, and modelling of the microphysical processes that strongly influence contrail formation and persistence. The model is similar to the MP model in that a chemistry module is simulated in a number of concentric rings which have differing concentration fields, that decrease with increasing radial distance from the plume core. The rest of the computation (i.e. mixing and microphysics) is peformed on a high-resolution Cartesian grid [48]. The primary aim of this model development was to bridge the gap between the simplified Gaussian approximation and more comprehensive large eddy simulations, as elaborated on in the following subsection.

### 3.2.4. Large eddy simulations (LESs)

Finally, the plume dynamical evolution can be most accurately captured using high-resolution LESs over the entire lifetime of the plume. LESs can model dynamics on a scale of several millions of grid points for a few seconds to a few minutes of plume age, providing unmatched levels of accuracy at the cost of extremely high computational demand. For this reason, LESs are usually limited to case studies from which the data obtained can be used to derive and calibrate plume parametrisations for use in the lower fidelity methods [49].

In Dürbeck and Gerz (1995) [44], LES data are used to calculate effective diffusion coefficients and plume cross-sectional properties for plume modelling purposes. The data obtained from the simulations is said to have agreed with Schumann et al. (1995) [40], where the horizontal and vertical plume scales and respective diffusivities are estimated from experimental data captured by a research aircraft measuring NO concentrations. Moreover, LESs have been used to determine plume properties on much

shorter timescales in Unterstrasser et al. (2014) [39]. In this paper, plume evolution is analysed for the jet and vortex period up to 6 minutes, whilst aircraft-induced dynamics dominate; concentration profiles and plume cross-sectional areas are determined for a range of atmospheric conditions, varying stratification, turbulence, wind shear and aircraft properties. Similarly in Paoli (2008) [50], detailed LES numerical simulations are carried out for the jet and vortex phase, confirming hypotheses surrounding aerosol and microphysics modelling. These studies exemplify the use of LES methods to validate experimental findings, and serve as a means of calibration for plume model parameters that represent real-life plume dilution characteristics.

## 4. Air traffic and emissions distribution

The previous section discussed the forces of flight and the generation and dispersion of aircraft emissions, from the perspective of a single aircraft. However, the state of the atmosphere is inhomogeneous with respect to space and time, meaning that the climate sensitivity to aircraft emissions differs considerably, depending on the time and location of their release. Furthermore, in airspace regions where traffic density is high, aircraft fly in close proximity and their exhaust plumes may intersect, giving rise to nonlinear local climate effects that must also be considered in aviation climate analysis. Therefore it is useful to explore the influence of air traffic management and spatial and temporal demand on the distribution of air traffic, and hence its associated emissions.

### *4.1. Air traffic management*

Air traffic management (ATM) is the system of services responsible for overseeing the network-wide implementation of safe, orderly and efficient air traffic flows, providing assistance to aircraft in transit from departure to destination aerodrome. It is the role of the air traffic control (ATC) team to manage and monitor air traffic in their respective airspace in real time, ensuring that optimum safety, order and efficiency of aircraft operations are maintained at all times [51].

#### 4.1.1. Air traffic safety

The inherent risk involved in the transportation of vast numbers of passengers at near transonic speeds through the upper atmosphere means that aviation safety is of paramount importance. A safe aircraft operation takes the path of least danger, primarily influenced by the need to avoid unfavourable atmospheric conditions and to prevent conflicts with other aircraft [52,53]. In-flight atmospheric conditions susceptible to icing, turbulence or the presence of hazardous convective weather can all be classified as unfavourable for aircraft, with the latter presenting the greatest constraint on aircraft routing [54,55]. The enhanced risk resulting from flight through weather-affected regions means that aircraft must re-route, leading to restrictions on available airspace and deviations from the optimal flight profile, thus increasing flight-times, fuel burn and delays [56].

The safety risks associated with aircraft-to-aircraft collisions necessitate air traffic controllers to impose safe separation standards between aircraft in the lateral, longitudinal and vertical direction, as specified in [57]. The stated minimum separation distances between aircraft are 5 nautical miles (NM) laterally, 20 NM longitudinally and 1,000 ft in the vertical direction under the most lenient scenarios. A breach of separation laws in more than one direction is known as a conflict and must be resolved as quickly as possible. The enforcement of separation minima therefore introduces a theoretical upper limit on airspace density, i.e. the number of aircraft that occupy a fixed volume of airspace at any one time.

#### 4.1.2. Air traffic order

To keep air traffic flows organised within controlled airspace, aircraft are ordered to follow the traditional fixed-route air traffic network, constructed from four key airspace elements that facilitate the air traffic management process [51]:

- **airports/aerodromes** - an area of land or water intended to be used for the arrival, departure and surface movement of aircraft;
- **waypoints** - a specified geographical location used to define the flight path of an aircraft, representing either a navigational aid (navaid) or a reference coordinate that the aircraft must fly-by or fly-over;
- **airways** - a controlled portion of airspace established in the form of a corridor (usually 8-10NM wide) between two waypoints;
- **sectors** - a region of airspace managed by a single ATC team, stratified into various levels to accommodate a wide variety of traffic.

In [58], the notion of optimising air traffic flows for a given demand and capacity is explored, in which air traffic flows are represented using these four key elements. **Airports** represent the sources and sinks of the flow, **airways** are the arcs along which the flow travels, **waypoints** are the network nodes at which airways intersect, merge or diverge, and **sectors** are a collection of waypoints and contiguous segments of airways. The fixed-route network restricts airspace availability even further, due to the discretisation of flight levels and the requirement to pass specified waypoints [59,60]. This can lead to particularly high frequencies of aircraft passing through high-density airspace, potentially leading to congestion along busy airways and waypoints where airways intersect resulting in inhomogeneities in the distribution of air traffic and potential congestion along high-density airways.

#### 4.1.3. Air traffic efficiency

The third and final component of effective air traffic management is the optimisation of flight trajectories, subject to the prioritisation of safety and the compliance with the fixed-route airspace structure. Flight trajectory optimisation is an essential step in ensuring maximum airspace utilisation and efficiency, so that revenue is maximised and demand levels are sufficiently met. Trajectory optimisation is a multi-faceted problem, requiring consideration of nonlinear aircraft performance, wind and weather forecasts, payload, departure fuel load, reserve fuel load and ATM constraints that restrict aircraft operations and routing [61]. This requires an exhaustive assessment to be carried out at the flight planning stage, to test all possible combinations of route, payload, fuel load and operating approach, involving tens to hundreds of thousands of calculations per flight. The most optimal scenarios are then ranked in order of optimality, with the final route selected based on operator preference and/or the occurrence of unexpected circumstances, such as sudden adverse weather conditions or aircraft conflicts [62].

In an ideal airspace situation where the atmosphere is calm and constant; aircraft are not constrained to a fixed route; and there is no risk of conflict with other aircraft, the least-time and least-energy aircraft operation would be to fly the great-circle arc between departure and destination. The vertical profile of the aircraft would consist of a continuous climb out to the most efficient cruise altitude, then to cruise at constant speed, with the ability to cruise-climb continuously as the aircraft burns fuel and loses mass. In reality, the true optimal route can deviate considerably from the great-circle arc, instead taking the path which minimises the risk of bad weather encounters and collisions, abides by the fixed-route airspace structure, whilst also flying a route which is optimised with respect to wind and temperature. The magnitude and direction of wind and the localised variation in temperature experienced by the aircraft throughout flight, can have a drastic impact on route optimality, with tailwinds and colder temperature regions being favourable [63]. Ng et al. (2012) [64] found for a wide range of wind-optimal flight scenarios that domestic flights saved up to 3%, and international flights saving up to 10% on both fuel burn and travel time, despite flying longer routes. Furthermore, the

vertical flight profile of the aircraft must adhere to flight level allocations, meaning that step climbs must be performed as fuel is burnt, further condensing air traffic and its corresponding emissions into narrow bands of altitude.

#### 4.1.4. Airspace capacity

The effective management of air traffic relies on the human cognition of air traffic controllers to make difficult decisions and carry out complex tasks in a time-critical dynamic environment. This includes ensuring safety through avoidance of poor atmospheric conditions and conflicts with other aircraft, maintaining order by flying along the fixed-route airspace network, and optimising air traffic flows with respect to wind and weather. As density and complexity levels of air traffic increase, so does the mental workload of the air traffic controller, up until a threshold level is reached where the controller can no longer safely handle the situation. The maximum number of aircraft permitted by the ATC team in charge of a particular airspace volume is known as the airspace capacity, and is driven by the airspace situation, state of equipment being used, and the controller's own mental state [65]. Airspace capacity is limited more by controller workload than is it separation laws, meaning human cognition is the true limiting factor on the number of aircraft that can occupy a particular airspace volume at a particular time [59,66]. Therefore, models of controller workload are often used to estimate airspace capacity, in which ATC tasks are modelled to determine a safe upper limit on workload. In Welch et al. (2007) [66], a macroscopic workload model is proposed which generalises ATC tasks into four distinct categories: background, transition, recurring and conflict tasks. This provides an objective basis for estimating capacity and enables the formulation of an analytical relationship between airspace capacity and sector volume, as seen in figure 7.

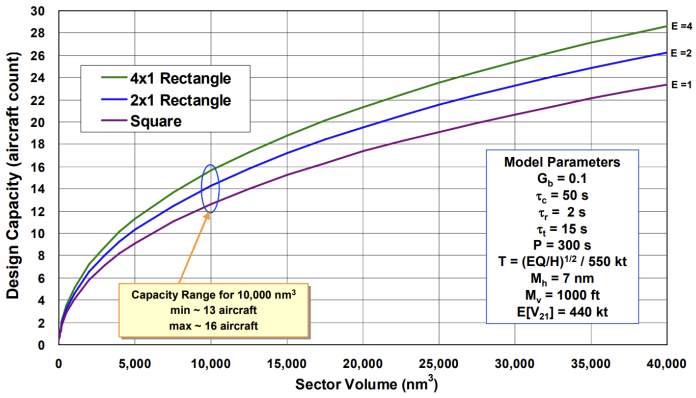


**Figure 7.** Aircraft capacity estimation against sector volume for a range of airspace scenarios [66].

The capacity estimation model from figure 7 predicts that, for a 10,000 $NM^3$ rectangular sector of dimensions 156 NM (length, ratio 4:1) $\times$ 39 NM (width) $\times$ 10,000 ft (height), a maximum of 16 aircraft may be present at any one time. In a purely hypothetical situation where separation laws dictate capacity and all aircraft are travelling in one direction lengthways, the sector could support a maximum of 490 aircraft, assuming a separation of 5 NM laterally, 20 NM longitudinally and 1,000 ft vertically. This emphasizes the sheer extent to which human factors limit the ability to maximise capacity, and highlights the need for airspace modernisation to increase automation, integration and collaboration in the ATM system, enabling the further increase in capacity levels towards minimum separation capacity [67].

### *4.2. Global air traffic and emissions distribution*

The nature of air traffic and emissions distribution was investigated in Olsen et al. (2013) [68] where a range of global aircraft emissions datasets are compared (NASA-Boeing 1992, NASA-Boeing 1999, QUANTIFY 2000, Aero2k 2002, AEDT 2006 and avia-

tion fuel usage estimates from the International Energy Agency) to show distribution patterns in the latitudinal, longitudinal and vertical sense. Further to this, temporal variations with respect to both the diurnal (time of day) and seasonal (time of year) cycles are explored.

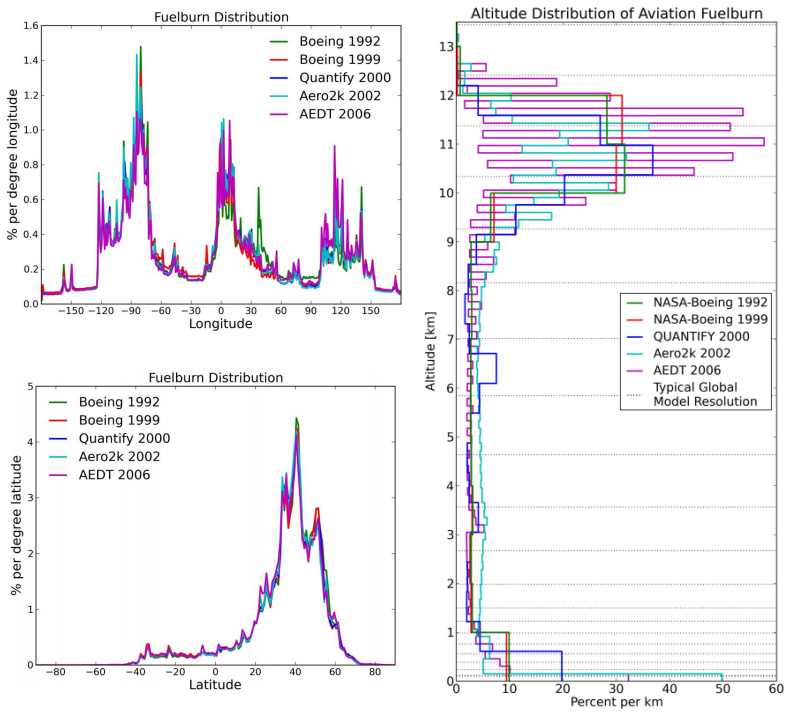


**Figure 8.** Spatial (latitude, longitude and altitude) distribution of global aviation fuel burn from a range of aircraft emissions datasets [68].

The climate sensitivity of the atmosphere is highly variable depending on the exact latitude, longitude and altitude combination, because of the spatially varying chemical and meteorological state of the atmosphere []. Accurate accounting of spatial distribution patterns of air traffic is therefore very important in the estimation of aviation climate impact. Figure 8 shows the spatial distribution of fuel burn across the range of datasets in the longitudinal, latitudinal and vertical directions. The longitudinal distribution shows three emissions peaks around the densely-populated regions of the US, Europe and East Asia, with the largest situated above the North American land mass. It is evident in the latitudinal distribution, that the Northern Hemisphere dominates, with a strong peak in the northern mid-latitudes that appears due to high volumes of air traffic above the US and Europe, as well as along the connecting region of airspace, the North Atlantic flight corridor (NAFC). Contrarily, there are almost no emissions present in southern latitudes below 40°S, with the region between 40°S and the equator constituting only a small percentage. The altitudinal distribution on the other hand, experiences emissions peaks around both the low altitude LTO area and the high-altitude cruising regions between 9 to 13 km, with relatively low emission intensities at mid-altitudes. Furthermore, the peak around cruising altitude is discretised into peaks every other flight level, due to the vertical separation constraints and the allocation of aircraft to specific flight levels, thus owing to further increases in emissions intensities at these altitudes.

Similarly, Wasiuk et al. (2016) [31] derived global $NO_x$ emissions totals for 2005 to 2011 by coupling an aircraft emissions modelling framework with an air traffic dataset for this period. Aircraft performance was modelled for each flight in the dataset using the BADA3 method [23] and the emissions were calculated using the BFFM2 [29]. Figure 9 portrays the spatial distribution of $NO_x$ emissions on a latitude-longitude map averaged over the six year period. For both altitude bands, main areas of aviation activity such

as flights over mainland and popular flight corridors are highlighted. The outcome of this analysis suggests similar findings to that of Olsen et al. for both the latitude and longitude plots in figure 8. In the longitude plots in figure 9, the three main areas of activity remain prominent; mainland US, Europe and East Asia, along with the much more distinguishable flight corridors that connect these regions. In the latitude plots, the Northern Hemispheric skew is also present, with most air traffic remaining within 20 to 60°N and a peak occurring around 40°N.

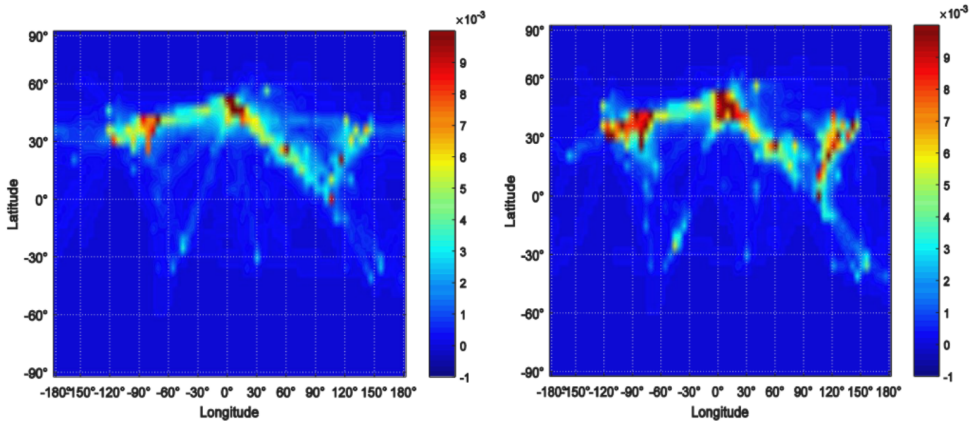


**Figure 9**

The presence of diurnal and seasonal variations in key chemical and meteorogical parameters throughout the atmosphere has been widely investigated in the literature []. The diurnal and seasonal variation in aviation fuel burn in figure 10 from Olsen et al. (2013) [68]. The temporal fluctuations in both the state of the atmosphere and the distribution of fuel burn and emissions allude to the fact that the climate sensitivity to aircraft emissions is always changing, and therefore these parameters must be under constant observation to ensure accurate determination of global climate effects from aviation. The diurnal cycle of global aviation fuel burn, as seen on the left hand side of figure 10 displays a peak at around 15:00 UTC, which decreases through the night until around 09:00 UTC where total fuel burn begins to increase again. With regards to seasonal variation, there is significant variance between emissions datasets, however in general, all display a wintertime minimum between December and January, and a summertime maximum between June and September.

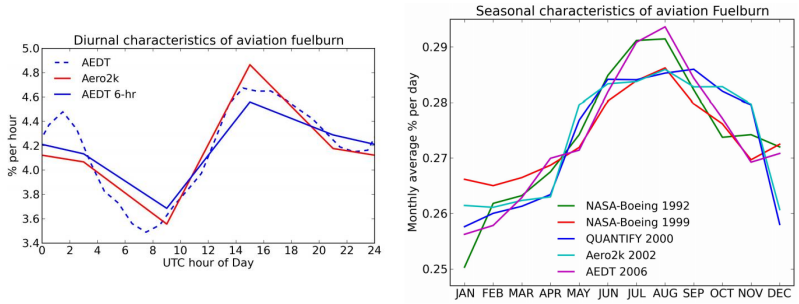


**Figure 10.** Temporal (diurnal and seasonal) distribution of global aviation emissions from a range of aircraft emissions datasets [68].

### *4.3. Local air traffic and emissions distribution*

Due to the fixed-route nature of airspace, aircraft tend to fly along common airways or flight corridors, and pass common waypoints along their journey, leading to exceptionally high flux densities of aircraft through these regions at peak times. This has

implications on the nonlinear chemical and physical effects occurring at the plume scale, due to the intersection of aircraft plumes and the elevated exhaust gas concentrations entrained within them. A prime example of a high-density airspace region is the NAFC, made up of a series of tracks that aircraft traversing the North Atlantic must follow, updated daily to allow for convective weather avoidance, tracking of the North Atlantic Jet Stream and favourable tailwinds to maximise efficiency [69]. The annually-averaged number of aircraft traversing the NAFC per day has increased from 800 in 1997 [70] to around 2,500 in recent years [71], owing to the tripling of passenger demand since then [72]. With North Atlantic air traffic being confined to a limited number of tracks (usually 3 or 4), it can be assumed that aircraft separation distances and airspace capacities are pushed to their limit on a regular basis along this and other popular flight corridors around the world.

Previous experimental work on air traffic emissions in the NAFC was carried out in the late 1990's, through campaigns such as the Pollution from Aircraft Emissions in the North Atlantic Flight Corridor (POLINAT) and Subsonic Assessment Ozone and Nitrogen Oxide Experiment (SONEX) [73]. At least 20 follow up papers were published following these campaigns, in which POLINAT/SONEX data are utilised to provide insight on a number of major scientific issues [74]. A noteworthy publication with regards to localised emissions impacts is [8], which carries out an in-situ investigation of air traffic emissions signatures (nitrogen oxides ($NO_x$), sulfur dioxide ($SO_2$) and cloud condensation nuclei (CCN)) in the NAFC using experimental data from a POLINAT research flight. The research aircraft flew perpendicular to the major eastbound corridor tracks and took measurements of various chemical concentration fields and meteorological parameters throughout. The results show that the superposition of aircraft exhaust plumes led to peak concentrations of $NO_x$, $SO_2$ and CCN above background levels by factors of 30, 5 and 3, respectively. This is because plume dispersion timescales greatly exceed the daily frequency with which aircraft emissions are input into the flight corridor, resulting in an inhomogeneous concentration field with narrow and sharp peaks over a relatively low and smooth background level [73].

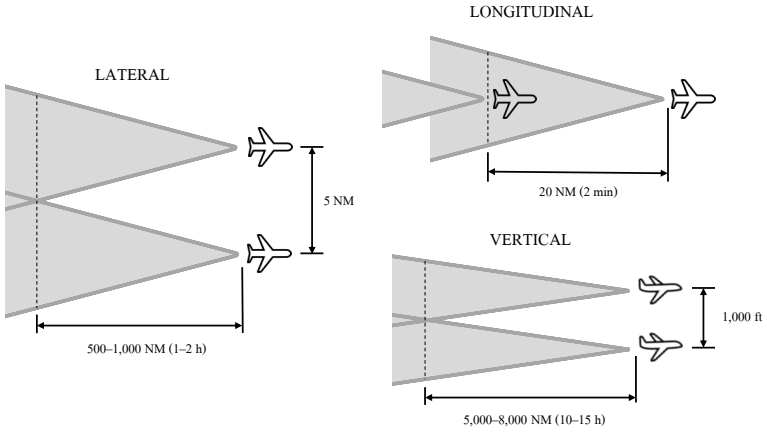


**Figure 11**

In the observation of plume-scale climate effects in high-density airspace regions, aircraft separation minima determine the minimum possible distance between aircraft and hence the maximum possible overlap between aircraft exhaust plumes. The degree of plume overlap influences the magnitude of emissions saturation, further accentuating nonlinear plume-scale climate processes that occur, as elaborated on in section 6. Using plume dimension estimates from Kraabol et al. (2000) [3], maximum plume overlap scenarios can be inferred. Figure 11 displays the lateral, longitudinal and vertical maximum overlap scenarios for aircraft cruising at 550 kt. The longitudinal separation

scenario proves to be the most effective formation for superimposing aircraft plumes, with the intersection time simply equalling the time taken to travel the separation distance between the two aircraft. For lateral and vertical superposition, the intersection time is much longer, as it is determined by the plume expansion rate in that particular direction, up until the midpoint between the two aircraft is reached. For lateral plume overlap to occur, the plumes must expand horizontally to a radius of 2.5 NM (15,190 ft), whereas for vertical, the distance is a mere 500 ft. Despite the drastic reduction in distance, the vertical plume overlap takes about an order of magnitude longer than lateral, because vertical plume expansion is substantially suppressed in comparison due to stable stratification counteracting vertical motions [40]. In reality, air traffic flows are much more complex and the controlled and orderly formations shown in figure 11 are unlikely to occur naturally. However, the premise still holds that plume overlap occurs most frequently in congested flight corridors such as the NAFC, when aircraft travel along similar tracks and the vertical displacement between aircraft is minimal.

The importance of safety, order and efficiency in the air traffic management process and the characteristics of global and local air traffic flows have been discussed. As the following section will explore, the atmospheric response to aviation emissions is highly sensitive to time and location, because the instantaneous state of the atmosphere (i.e. the chemical composition and meteorological situation at that particular time and position) determines the production, loss and radiative response of key chemical species that induce climatic effects [32]. With insight into how air traffic and emissions are dispersed locally and distributed globally, the contribution of aircraft emissions to climate change can be more rigorously evaluated.

## 5. The climate impact of aviation

Aircraft emissions induce climate effects by perturbing the flux of inbound shortwave (SW) solar radiation and outbound longwave (LW) terrestrial radiation emitted from the Earth's surface through absorption and scattering processes that give rise to warming or cooling of the atmosphere [75]. Climate metrics such as radiative forcing can be used to measure the climate contribution of each individual emission species, enabling the determination of the net global warming effect from aviation. Accurate quantification of aviation's climate impact requires sufficient modelling of plume-scale effects that are neglected in global models. The accumulation of aircraft emissions in high-density flight regions can lead to saturation effects which affect aviation's net warming effect. This section elaborates on the literature associated with these research areas, to help the reader conceptualise why the atmospheric response to aircraft emissions is dependent on background ambient conditions, and hence why it is also influenced by the presence of other aircraft exhaust plumes in close vicinity.

### *5.1. Aircraft emissions in the Upper Troposphere and Lower Stratosphere*

As figure 8 suggests, the vast majority (~60%) of aviation fuel burn and hence aviation emissions, occur at cruise altitudes, between 9 and 13km vertically. The region of the atmosphere encompassing this volume of airspace is known as the Upper Troposphere and Lower Stratosphere (UTLS), with bounds of $\pm$5 km above and below the conventional tropopause [76]. Around 20-40% of total aircraft emissions are released in the LS [14**?** ] and the rest are released in the troposphere, extending from the surface at take-off to the UT at aircraft cruise altitudes. The greenhouse effect due to the release of chemically-active substances in the UTLS is considerably greater than that of emissions at the surface. This is because the climate in the UTLS is more sensitive due to increased residence times of pollutants, lower background concentrations (meaning emissions have a greater influence on the atmospheric chemistry), lower temperatures, and a higher radiative efficiency [77]. Johnson et al. (1992) [78] further validates this claim, with model results concluding thaty $NO_x$ emissions constitute a 30 times greater climate

impact in the UT compared to equivalent surface emissions, due to the absence of direct deposition and slower conversion to stable reservoir species at aircraft cruising altitudes.

Brief description of atmospheric situation in the UTLS:

- atm trace species present,
- oxidative capacity of the atmosphere and radical chemistry,
- photochemistry and the climate relevance of ozone etc.
- temperature profile,
- ozone profile,
- methane profile,
- water vapour profile,
- STE.

Despite such as large proportion of air traffic being released into the LS region, it is thought that the perturbation to the chemical and radiative state of the stratosphere is negligible, as the vast majority of species emitted into the stratosphere are transported downwards into tropospheric regions, where they perturb the atmosphere there [79–81]. Henceforth, this review will primarily focus on the tropospheric response to aircraft emissions, except for water vapour, where the stratospheric climate response becomes particularly noteworthy.

### *5.2. Radiative forcing of aircraft emissions*

High altitude emissions from aviation impact the climate through a variety of climate forcing pathways. Some greenhouse gases such as $CO_2$ and $H_2O$ are emitted directly, others are produced indirectly through chemical processing of aircraft, such as the reaction of $NO_x$ with atmospheric trace species to catalyse ozone production and methane destruction. Water vapour and particulate matter (PM) emissions are responsible for the formation of high ice clouds known as condensation trails (contrails), which often trap outbound LW radiation within the atmosphere more efficiently than they reflect inbound SW radiation. PM emissions also have the potential to induce a climate perturbation through direct radiative processes due to aerosols, which may warm or cool the climate depending on the particle's optical and microphysical properties [79]. Diversity in the climate forcing pathways for each emission species means that the only reliable method of determining the severity of each climate contribution is to model the atmospheric response and determine the resulting impact on the radiative flux of the atmosphere [7].

The most common climate metric used to compare the magnitudes of climate impact from a range of emission species is radiative forcing (RF). RF is defined as the perturbation to the net energy balance of the Earth-atmosphere system due to natural or anthropogenic factors of climate change, measured in watts per square metre [$Wm^{-2}$] [82]. Climate forcers such as greenhouse gases and contrails A positive RF means that the climate forcing mechanism is inducing a warming effect and vice versa. Lee et al. (2021) [1] presents an updated analysis of the global effective radiative forcing (ERF) contributions for aviation-induced climate change. ERF is a newly proposed climate modelling framework that builds upon the RF concept by removing rapid atmospheric adjustments that bear no relation to the long-term surface temperature response that occurs over decadal timescales [75]. ERF serves as a more suitable equivalency metric to compare the global warming response of heterogeneously distributed short-lived climate forcers and uniformly distributed long-lived climate forcers. Figure 13 displays the ERF and RF contributions for each of the key aviation-induced climate forcers.

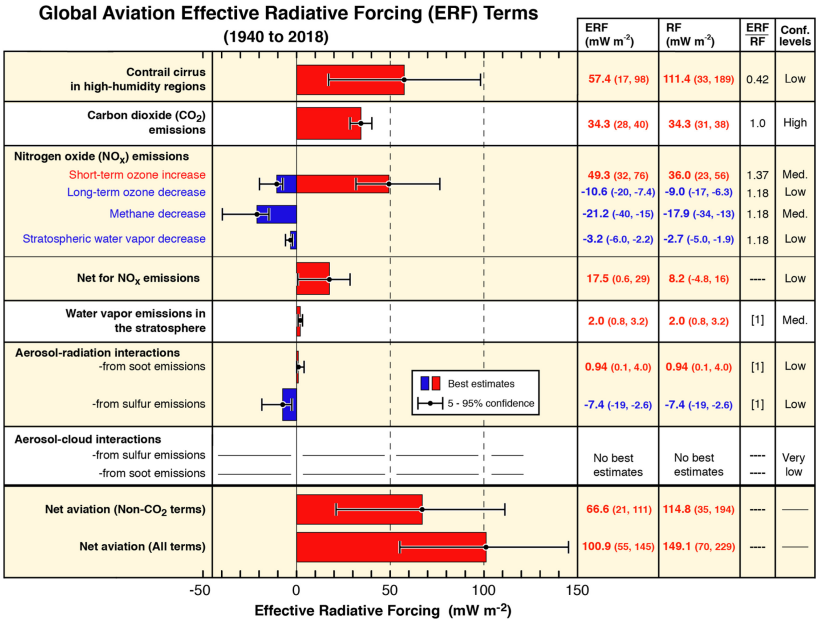


**Figure 12.** Radiative forcing contributions from global aviation between 2000 and 2018 [1].

### 5.2.1. $CO_2$

The climatic effects of aviation $CO_2$ emissions are direct and well understood, with the thermal absorption of outbound LW radiation leading to warming through the planetary greenhouse effect [83]. Carbon dioxide from aircraft constitutes the second largest ERF term in figure 13 at 34.3 $mWm^{-2}$, and the thermodynamic and photochemical stability of $CO_2$ means it has a relatively long atmospheric lifetime, on the order of 100 to 1,000 years [84]. This means that carbon emissions from aircraft simply serve to increase its atmospheric concentration, leading to the eventual distribution over global spatial scales. The ubiquitous and intuitive nature of $CO_2$-related warming deems it a suitable benchmark to compare warming from non-$CO_2$ climate forcers against. The assumption of instantaneous dilution in global models is sufficinet for modelling the climate impact due to carbon dioxide, as it exists over vast spatial and temporal scales, meaning the climatic effects occurring on plume time scales are negligible compared to the impact induced over its entire lifetime [5].

### 5.2.2. Contrail cirrus

When emissions of water vapour and PM are released into the aircraft exhaust plume in the cold and moist condition of the UTLS, the water vapour condenses around the particulates due to the high relative humidity (RH), then freezes due to the low external temperatures, permitting the formation of ice crystals. The accumulation of ice crystals in the aircraft wake gives rise to the generation of a condensation trail, also known as a contrail. Contrails have a significant level of opacity and occur at high altitudes, tending to absorb outbound terrestrial radiation more efficiently than they reflect inbound solar radiation. This induces a globally averaged ERF of (57.4 $mWm^{-2}$), meaning, despite their relatively short lifetime in comparison, the current contrail effect contributes more to climate change than the accumulation of aviation carbon since the dawn of aviation [85]. Contrail evolution, i.e. how it grows, disperses and persists with time, is largely determined by the ambient conditions of the surrounding atmosphere, with lower temperatures and higher humidities generally leading to a more persistent and damaging contrail [86]. The formation and persistence of contrails can be predicted purely from the thermodynamic assumption that, as the hot and moist exhaust mixes with the colder and drier ambient air, a contrail will form if the plume exceeds water-saturation at any point and the temperature is low enough for ice nucleation to occur.

A contrail will persist in the atmosphere if it mixes with air that is supersaturated with respect to ice, i.e. an ice-supersaturated region (ISSR) [2].

The thermodynamic constraints for contrail formation and persistence were first theorised by Schmidt (1941) [**?** ] and Appleman (1953) [87], based on prior empirical observations [88], that led to the promulgation of the so-called "Schmidt-Appleman (SA) criterion". The SA criterion shows that the contrail formation threshold is purely dependent on ambient pressure, relative humidity, and the ratio of water and heat released into the exhaust plume, assuming isobaric mixing between exhaust emission and full dilution into the ambient atmosphere [89]. See Tait (2020) [90] for a detailed description of how the SA criterion can be illustrated on a plot of water vapour partial pressure against temperature. Contrails which surpass water saturation, but do not settle in ice-supersaturated air are generally assumed to be short-lived, as the ice sublimates and deposits into the surrounding atmosphere. Contrails released into ISSRs however, tend to persist as they uptake surrounding water vapour and grow with time. Persistent contrails can sometimes transition to contrail cirrus, either building onto existing cirrus clouds or forming new ones, spreading over vast swathes of the atmosphere and inducing significant radiative effects. ISSRs occur frequently at aircraft cruising altitudes and often span hundreds of kilometres horizontally, however only reach depths of 100 to 1,000 m [91,92]. Their shallow nature means that aircraft can avoid them by changing flight level by $\pm$2000 ft to minimise persistent contrail generation for a minor additional fuel penalty [93].

Contrails exhibit radiative forcing through the obstruction of both SW and LW radiative fluxes, with areal coverage and optical depth being the key drivers of contrail climate impact [94]. A contrail's emissivity (ability to absorb and re-emit infrared LW radiation back towards Earth) and reflectance (ability to reflect inbound SW radiation back out to space due to scattering at visible wavelengths) is a function of contrail optical depth and ice particle microphysics. Contrails and other high ice clouds often warm the climate, as their thin optical depth means partial transparency to solar radiation, whilst their high ice density traps infrared radiation within the atmosphere effectively [2]. Contrail RF also displays a distinct diurnal trend; at night, contrails always induce a warming effect, as there is no SW scattering to counteract the LW absorption. During the day, contrails display a reduced net warming effect and perhaps even a net cooling effect, depending on the amount of solar radiation that is redirected back out to space [95]. The SA criterion can be used to predict formation and persistence of contrails, however accurate quantification of contrail RF requires sufficient microphysical modelling, to deduce key information on the underlying formation mechanisms and physical and optical properties the contrail exhibits throughout its evolution [96]. See section 5.3.3 for elaboration on the microphysical processes that determine a contrail's radiative characteristics, and how these processes can be parametrised for modelling purposes.

#### 5.2.3. Net-$NO_x$

Nitrogen oxides (NO and $NO_2$) released from aircraft are not radiatively active and therefore do not induce an immediate climate impact at the point of emission. Their chemical instability does however mean that they exhibit a number of indirect RF effects, due to the chemical reactions that occur following dilution into the ambient atmosphere. The chemical interactions between $NO_x$ and trace species in the background atmosphere at aircraft cruising altitudes are highly non-linear and thus, the net-$NO_x$ RF contribution is dependent on the instantaneous atmospheric state (time of day and year, latitude, background chemical composition, meteorological situation).

Emissions of $NO_x$ in the troposphere initially leads to the short term increase in ozone production efficiency ($O_3$) on the time scale of weeks to months. In addition, elevated $NO_x$ and $O_3$ levels lead to increased hydroxyl radical (OH) production, which in turn, leads to the long term destruction of ambient methane ($CH_4$) over the time scale of decades [97–99]. The short term increase in $O_3$ generates a strong positive ERF

of 49.3 $mWm^{-2}$, whereas the long term $CH_4$ depletion causes a lesser negative ERF of -21.2 $mWm^{-2}$ in comparison, however there are a number of secondary negative radiative effects arising from methane depletion that must also be accounted for. This is the reduction in stratospheric water vapour (15% $CH_4$ RF magnitude) and a decrease in long-term background ozone in the troposphere (45% $CH_4$ RF magnitude), resulting from reduced background $CH_4$ concentrations [100,101]. Despite the long-term negative cooling effects, the short term warming from $O_3$ dominates, leading to a largely positive net ERF of 17.5 $mWm^{-2}$ overall, as seen from figure 13. Section 5.3.1 explores the nonlinear $NO_x$-$O_3$ relationship further through explanation of the gas-phase photochemical processes that begin in the aircraft plume and are eventually distributed to regional and global scales.

Spatial scales of NOx impacts - is short term ozone warming a local effect, whereas methane acts globally due to longer diffusion time?

#### 5.2.4. Water vapour

The direct radiative effects induced by aviation water vapour emissions in the troposphere are insignificant, because the influence on background concentrations is negligible compared to the natural fluxes of the Earth's hydrological cycle [14]. Any tropospheric water vapour emissions tend to get lost through deposition, due to high humidity and precipitation in this region, leading to a lifetime of around 9 days. On the contrary, water vapour that is emitted into the stratosphere (without getting transported downwards into the UT) can induce a considerable effect on the surrounding environment, due to extreme dryness at these altitudes [].

Strat water vapour:

- Why it leads to warming in the Strat - greenhouse effect? Also, chemical loss of ozone due to increased PSC?
- Total climate effect of SWV from (Lee2021) - ERF of 2.0 $mWm^{-2}$.
- Potential for much larger impact in future due to HSCT flying in strat and hydrogen aircraft (Lee2010).

#### 5.2.5. Aerosol effects

Aviation aerosol particles, either emitted directly post combustion, or formed in the wake of the aircraft, can perturb the energy balance of the atmosphere directly, as well as indirectly through the formation of contrail ice particles and heterogeneous chemical processing. The direct aerosol effect is primarily produced by the key non-volatile and volatile PM emissions; soot and sulphate aerosols.

Soot exhibits a direct radiative forcing as it has the strongest absorption of light at visible wavelengths per unit mass, more than any other abundant substance in the atmosphere, thus contributing to global heating through absorption of inbound solar radiation and light rebounded off reflective surfaces such as snow and ice [102]. The resultant heating of the atmosphere and reduction of sunlight can affect the hydrological cycle and large-scale circulation patterns, having potentially larger implications on the climate than previously thought. Despite its ability to strongly absorb sunlight, aircraft soot is responsible for only a few percent of total atmospheric black carbon meaning the aerosol-radiation interaction brought about by aviation soot only constitutes a minor ERF of 0.94 $mWm^{-2}$.

Sulphur dioxide ($SO_2$) is formed when sulphur, which is present in hydrocarbon jet fuels, oxidizes during the combustion process [103]. Emitted $SO_2$ can then form sulphuric acid ($H_2SO_4$) and further oxidation to sulphate aerosol particles ($SO_4$) in the presence of water vapour []. The optical properties of sulphate mean that it tends to scatter inbound sunlight, thus leading to a net negative (cooling) $mWm^{-2}$, that sways the net direct climate impact of aviation aerosols towards cooling.

It is relatively well established that aviation-induced aerosols have a direct impact through radiative interactions, as discussed in this section, as well as indirectly through

activation of water vapour on PM emissions through contrail formation. There are however, potentially large indirect consequences of aerosol particles interacting with cloud droplets and ambient ice particles nucleation on the aerosol surface. These effects are left without ERF estimates in figure 13, as there is great uncertainty around the accuracy of cloud process modelling [104].

### *5.3. Nonlinear plume-scale climate effects*

As detailed in the previous section, the global contributions to aviation radiative forcing have been relatively well quantified. However, much of the modelling processes used to estimate these contributions are derived from global models assuming instant dispersion, thus excluding subgrid-scale chemical and physical effects that occur in the first 2–12 h upon release into the atmosphere. This section reviews current scientific understanding of these plume-scale processes, and highlights their emerging relevance in increasingly high-density airspace regions, as the accumulation of chemically active emission species further propagates the nonlinear climate response.

#### 5.3.1. Gas-phase photochemistry

Gas phase photochem:

- Intro explaining why ozone is formed in ambient atmosphere (Oxidation of CO?).
- Role NOx has to play in this (Jaegle1999, Wasiuk2014, Freeman2017).
- Definition of all species mentioned and the role they have to play in ozone formation (M, nu, HOx, R, R-H etc.).
- Maybe a chemical explanation of why methane is oxidised, with relevant reactions mentioned?
- Hint at potential for NOx-saturated conditions in atm (Lin1988).
- Explain what reactions are not properly accounted for in global modelling (NO titration etc.) - three chemical regimes from (Fritz2020).

In the early stage of plume dilution (first 10 minutes), when $NO_x$ concentrations are very high, ozone titration by NO results in a large production of $NO_2$ but decreases the formation of $HO_2$ and OH because of depleting ozone levels in the plume. The reduced ozone is partly compensated by $NO_2$ photolysis.

$$NO + O_3 \longrightarrow NO_2 + O_2 \tag{R1}$$

The dilution of the plume results in low $NO_x$ concentrations which can be oxidized by peroxy radicals $HO_2$ and $RO_2$ (formed from the oxidation of CO and VOCs by OH) leading to $NO_2$ production that undergoes photolysis resulting in the production of ozone. The photolysis of ozone and subsequent reaction of $O(^1D)$ with water generates OH radicals.

$$NO + HO_2 \longrightarrow NO_2 + OH \tag{R2}$$

$$NO + RO_2 \longrightarrow NO_2 + RO \tag{R3}$$

$$NO_2 + h\nu \longrightarrow NO + O(^3P) \tag{R4}$$

$$O(^3P) + O_2 \longrightarrow O_3 \tag{R5}$$

$$O_3 + h\nu \longrightarrow O_2 + O(^1D) \tag{R6}$$

$$O(^1D) + H_2O \longrightarrow 2\,OH \tag{R7}$$

OH formed from the reaction (R2) and reactions (R6) to (R7) react with CO and VOCs to form peroxy radicals which propagate reactions (R2) and (R3) and can enhance ozone production.

$$CO + OH \longrightarrow CO_2 + H \tag{R8}$$

$$H + O_2 + M \longrightarrow HO_2 + M \tag{R9}$$

$$R{-}H + OH \longrightarrow R + H_2O \tag{R10}$$

$$R + O_2 + M \longrightarrow RO_2 + M \tag{R11}$$

However, OH can also react with NO and $NO_2$ to form nitrogen reservoir compounds such as nitrous acid (HONO) and nitric acid ($HNO_3$), which remove radicals from the atmosphere and prevent further ozone formation.

$$NO + OH + M \longrightarrow HONO + M \tag{R12}$$

$$NO_2 + OH + M \longrightarrow HNO_3 + M \tag{R13}$$

Depending on the precursors' background concentrations (e.g. VOCs, CO), there are possibilities of the formation of some other reservoir compounds (e.g. $HO_2NO_2$, $RO_2NO_2$, PAN etc.) which also limit the formation potential of ozone in the exhaust plume.

$$NO_2 + HO_2 + M \longrightarrow HO_2NO_2 + M \tag{R14}$$

$$NO_2 + RO_2 + M \longrightarrow RO_2NO_2 + M \tag{R15}$$

$$NO_2 + RCO_3 + M \longrightarrow RCO_3NO_2 + M \tag{R16}$$

#### 5.3.2. Heterogeneous chemistry

Het chem:

- Brief definition of het chem (Jacob2000).
- Factors influencing het chem reaction rates (Meilinger2002, Meilinger2005).
- How het chem influences contrail formation - and how het chem is influenced by contrail formation (feedback loops?) (Meilinger2005, Lee2010).
- The impact of het chem on eventual O3 output and contrails, and how this has an effect on global RF (Refs - not so sure yet!).

The effect of plumes on atmospheric photochemistry is shown to increase the soot, sulphate and water-ice surface areas for heterogeneous reactions which are important in defining ozone removal rates in the UTLS.

$N_2O_5$ formed from the oxidation of NOx undergoes a reactive uptake on the plume species (e.g. water-ice surface), which results in $HNO_3$ formation. The reaction of $N_2O_5$ with HCl on ice results in $ClNO_2$ formation (R18) which can compete with heterogeneous hydrolysis of N2O5 (R17).

$$N_2O_5 + H_2O \longrightarrow 2\,HNO_3 \tag{R17}$$

$$N_2O_5 + HCl \longrightarrow ClNO_2 + HNO_3 \tag{R18}$$

The heterogeneous interactions are very important to the removal of $NO_x$ and $HO_x$ species during sedimentation events in the UTLS. These reactions can form reservoir species (e.g. $HNO_3$, $H_2O_2$) which can absorb onto sulphate aerosol and ice particles. Heterogeneous denoxification (reactions (R17) and (R18)) and dehoxification (reactions (R19) and (R20)) lead to a reduced concentrations of $NO_x$ and $HO_x$ which reduce the ozone production through gas-phase reactions [**?** ].

$$2\,HO_2 \longrightarrow H_2O_2 + O_2 \tag{R19}$$

$$2\,OH \longrightarrow H_2O_2 \tag{R20}$$

In the stratosphere, a number of heterogeneous reactions (R21) to (R29) are important to various degrees on the surface of ice particles and saturated ternary solutions of water, HNO3 and H2SO4 in terms of ozone depletion on a global scale.

$$ClONO_2 + H_2O \longrightarrow HOCl + HNO_3 \tag{R21}$$

$$ClONO_2 + HCl \longrightarrow Cl_2 + HNO_3 \tag{R22}$$

$$ClONO_2 + HBr \longrightarrow BrCl + HNO_3 \tag{R23}$$

$$HOCl + HCl \longrightarrow Cl_2 + H_2O \tag{R24}$$

$$HOCl + HBr \longrightarrow BrCl + H_2O \tag{R25}$$

$$BrONO_2 + H_2O \longrightarrow HOBr + HNO_3 \tag{R26}$$

$$BrONO_2 + HCl \longrightarrow BrCl + HNO_3 \tag{R27}$$

$$HOBr + HCl \longrightarrow BrCl + H_2O \tag{R28}$$

$$HOBr + HBr \longrightarrow Br_2 + H_2O \tag{R29}$$

The heterogeneous reactions initiated by $ClONO_2$, HOCl, $BrONO_2$, HOBr produce Cl2, BrCl, $Br_2$ which then yields Cl and Br radicals by photolysis. These heterogeneously activated Cl and Br can enhance ozone depletion (Meilinger et al., 2005).

The extent of heterogeneous reactions (R17) to (R29) offset the effects of gas-phase reactions (R1) to (R16) on $NO_x$ initiated ozone formation which depends on a variety of chemical and dynamic factors (e.g. aerosol microphysics, atmospheric dynamics).

#### 5.3.3. Microphysics

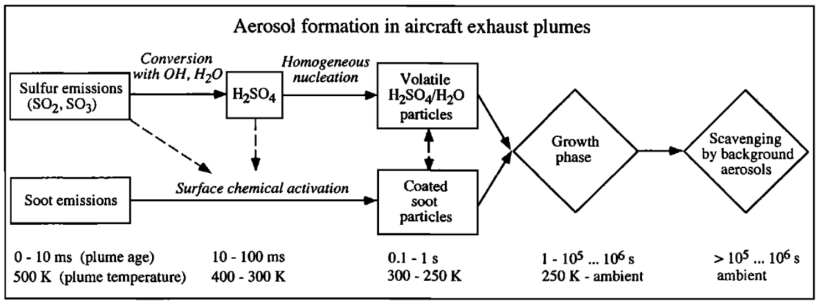


**Figure 13**

*5.4. The saturation of aircraft emissions in high-density airspace regions*

*5.5. Aviation climate modelling*

#### 5.5.1. Global climate modelling

Climate models provide a realistic quantitative estimate of future climate change especially at the continental scale. In recent years, various climate models have been developed to improve understanding of climate processes and to perform more realistic time-dependent simulations of climate change. These models can incorporate physical processes in greater complexity such as coupling of climate system components and enhanced model resolution. The most sophisticated climate models are the General Circulation Models (GCMs) coupled with the chemistry scheme which can be used to study the potential anthropogenic influences on current and future climate [**?** ]. However, the GCMs are very complex and computationally expensive, therefore may need very long processing time to run (depending on the climate perturbation) on a high-performance computer. To overcome this, simple climate models (SCMs) are used for estimating future climate impacts of aviation activity which are generally parameterized to reproduce the main characteristic responses of GCMs.

SCMs are known as reduced complexity model, computationally inexpensive and widely used decision support tools for the policy makers. SCMs are used to evaluate climate impacts from a wide range of sources, from total anthropogenic emissions to sectoral emissions (e.g., aviation emissions). Model for the Assessment of Greenhouse Gas Induced Climate Change (MAGICC) is one of the SCMs which is not specific to aviation and can be used in different emissions scenarios to estimate time-dependent concentrations, radiative forcing, temperature response and sea-level rise from different perturbations [**?** ]. Linear climate response model (LinClim) is a very effective SCM which has been customised specifically for aviation purposes. It implements a single impulse response function that is calibrated against more sophisticated parent GCM model. The global aircraft fuel emissions derived from emissions database and the calculated emissions indices are used to calculate historical, present day and future emissions trends of CO2, NOx, water vapour, sulphate and black carbon aerosols. LinClim calculates the climate impacts from non-CO2 species and contrails by scaling the emissions or distance travelled to an externally calculated base year radiative forcing. The carbon cycle in LinClim is based on the Maier-Reimer and Hasselmann (1987) [] model and the CO2 RF is calculated using the function applied in IPCC AR468 [**?** ]. The temperature response can be calculated by LinClim using radiative forcing and climate model parameters that are parameterized to LinClim's parent GCM.

The impact of the species released from aircraft on the atmosphere is non-linear. Thus, a non-linear climate-chemistry response model, AirClim $Grewe_{2008}$ applicable to aviation industries is developed. This model comprises a linearisation of atmospheric processes from the emissions and productions of $CO_2$, $H_2O$, $CH_4$, $O_3$ and contrails to radiative forcing, resulting in an estimate of surface temperature change.

The FAA Aviation Environmental Portfolio Management Tool (APMT) uses impulse response models along with a simplified energy balance model to give aviation impacts for CO2, NOx on methane, NOx on ozone, sulphates, soot and contrails/contrails cirrus in terms of radiative forcing and global temperature change [**?** ].

#### 5.5.2. Effective emissions and parametrisation of plume-scale effects into global models

Plume modelling methods serve as a useful tool for analysing the chemical and physical evolution of aircraft exhaust plumes throughout their lifetime. However, integrating high-resolution plume data into global atmospheric models is simply unfeasible when a large number of flights, on the order of 100,000-200,000 flights per day [], must be considered. To counteract this, simpler parametrisations of plume models are used, which capture so-called “effective emissions" that attempt to correct the ID response of the large-scale model, according to the predicted plume-scale effects and their influence on the eventual climate impact. Parametrising plume-scale climate effects into global atmospheric models that assume instantaneous dispersion is a topic covered extensively in the literature, for both ozone-$NO_x$ chemistry [5,34,105**?** ] and contrail and cloud processes [**?** ]. In [5], three key concepts are reviewed which enable the parametrisation of nonlinear plume chemistry into ID global models; effective emission indices (EEIs), effective conversion factors (ECFs) and effective reaction rates (ERRs).

EEIs are a concept first theorised in Petry et al. 1998 [33], in an attempt to account for the difference in concentration evolution of key chemical species between global models which assume emissions instantaneously disperse and plume models which account for the entrainment of emissions throughout the plume lifetime. EEIs provide a suitable correction to the original EI of an emitted species, so that the concentration is the same in the ID model as it is in the plume model, at the end of the plume "dispersion time" $t_{ref}$, when emissions are fully dispersed into the dimensions of the computational grid cell in which they were released.

Meijer (2001) [45] presents the concept of ECFs, which accounts for the chemical conversion of $NO_x$ to nitrogen reservoir species in the plume. This significantly affects the net chemical rates of $NO_x$ and $O_3$ once the plume is fully dispersed into ambient air. ECFs parametrise plume-scale effects by scaling the EI of $NO_x$ according to the ratio of emission species $i$ to the emission of total reactive nitrogen ($NO_y$) in the aircraft exhaust plume. Since the total emitted $NO_y$ is chemically conserved throughout the plume lifetime, the amount of $NO_y$ throughout the plume lifetime is equal to the amount of $NO_x$ emitted initially, and hence the sum of ECFs for $NO_x$ and all reservoir species is unity [43]. This means that due to the faster conversion of $NO_x$ to reservoir species within the plume, the ECF of $NO_x$ decreases, whilst the ECFs of reservoir species such as $HNO_2$ and $HNO_3$ increase considerably. The ECF of $O_3$ is

In ERRs, the concentrations of the emitted species in the plume can be reconstructed by diluting the emission to the size of the CTM grid-cell, while the modified reaction rates are used to model reactions with the non-emitted species

## 6. Aircraft exhaust plume superposition and the saturation of emissions

### *6.1. The saturation of Nox emissions and influence on photochemistry*

In 6, the notion of plume superposition and the extent to which it influences the atmospheric response was explored, by comparing results from an expanding plume model against an atmospheric model which assumes instant dilution. The analysis was carried out firstly on a single aircraft at cruise altitude, then on four aircraft flying in the same direction each separated by 1 hr. Observing the single aircraft’s plume 10 hrs after emission, it was found that the instantaneous dilution approach overestimated O3 production by 33%, CH4 destruction by 30% and CO destruction by 32%. When observing the response due to the four overlapping plumes however, the overestimation of O3 production increases to 77%, CH4 destruction to 68% and CO destruction to 74%. The marked difference in measured response for four overlapping plumes compared to

a single plume serves as evidence that emissions saturation in superimposed plumes can significantly alter the chemical response of the atmosphere. However, further work needs to be done to clarify the direction and magnitude of the net change in climate impact resulting from these changes to the chemical composition. Moreover, the sensitivity of the chemical and climate response to plume superposition needs to be tested for a range of aircraft transit frequencies and ambient atmospheric conditions, so as to build up a visual representation over the phase space of the atmosphere.

### *6.2. Dehydration of water vapour due to contrail formation*

In addition to chemical changes in the atmosphere, plume overlap can also influence the formation and persistence of aircraft contrails and the subsequent generation of aviation-induced cirrus clouds. 6 explored the effect of recurrent water vapour emission on contrail formation and persistence at typical aircraft cruising altitudes. It was discovered that continual contrail generation actually leads to dehydration of the surrounding atmosphere and a diminishing radiative forcing effect of 15% in the affected areas. This outcome provides further impetus to explore the potential effects of plume superposition on the global warming induced by aviation.

## 7. Operational mitigation strategies

This section explores the potential for operational mitigation procedures. These mitigation which utilise knowledge of the spatio-temporal variability in the atmospheric response to aircraft emissions,

### *7.1. Formation flight*

Formation flight involves the flight of two or more aircraft in aerodynamic formation, with the follower aircraft positioned in the smooth updraft of the leader aircraft's wake, reducing required lift and thrust, hence reducing fuel and CO2 emissions by 5-8% per trip 6. A fortuitous outcome of formation flight is however, the saturation of emissions in the trailing exhaust plumes, which can lead to the aforementioned nonlinear chemical and microphysical response that reduces ozone and contrail formation. The non-CO2 climate effects of a twin-aircraft formation flight are observed in 6, where a climate model was used to determine the changes in NOx-related ozone production and contrail formation processes. The case study found that, despite a 1-3% increase in flown distance, CO2 was reduced by 6% and NOx was reduced by 11%. This resulted in a 5% reduction in ozone production efficiency due to NOx saturation and a 48% contrail reduction due to mutual competition for available water vapour, resulting in a total climate impact reduction of approximately 23%. While part of the alleviated climate impact can be related to the decrease in total emissions due to wake energy retrieval of the follower aircraft, there is also further emphasis due to the saturation of emissions in the overlapping plumes of both aircraft involved. This demonstrates great potential for reducing both CO2- and non-CO2-induced climate effects from aviation, if such a scheme were to be carried out on a global scale.

### *7.2. Climate-optimal aircraft routing*

Fleet-wide implementation of formation flight would however, pose a number of research obstacles, that must be overcome to maximise its cost-benefit potential, whilst ensuring the safe and orderly operation of aircraft in controlled airspace. Optimising aircraft trajectories to minimise fuel burn requires the consideration of nonlinear aircraft performance, wind and weather, payload, fuel load, and constraints set out by air traffic control []. Formation flight adds another variable to the fuel burn optimisation problem, maximising the time spent flying in formation whilst minimising deviation from the true optimal route. This is a research topic covered extensively in the literature []. Optimising formation flight trajectories to minimise climate impact on the other hand, is a relatively

novel concept, which requires deeper understanding of the sensitivity of the climate response to emissions under a range of different atmospheric states.

Newinger and Burkhardt (2012) [95] explored the potential for mitigation of night-time contrail forcing through air traffic scheduling adjustments. They proposed...

Teoh et al. investigated the possibility of small-scale diversion of aircraft to avoid persistent contrail formation in most sensitive regions and achieved a ... reduction in contrail climate impact for a ... increase in ... .


1. Lee, D.; Fahey, D.; Skowron, A.; Allen, M.; Burkhardt, U.; Chen, Q.; Doherty, S.; Freeman, S.; Forster, P.; Fuglestvedt, J.; Gettelman, A.; De León, R.; Lim, L.; Lund, M.; Millar, R.; Owen, B.; Penner, J.; Pitari, G.; Prather, M.; Sausen, R.; Wilcox, L. The contribution of global aviation to anthropogenic climate forcing for 2000 to 2018. *Atmospheric Environment* **2021**, *244*, 117834. doi:10.1016/j.atmosenv.2020.117834.
2. Kärcher, B. Formation and radiative forcing of contrail cirrus. *Nature Communications* **2018**, *9*, 1824. doi:10.1038/s41467-018-04068-0.
3. Kraabøl, A.G.; Konopka, P.; Stordal, F.; Schlager, H. Modelling chemistry in aircraft plumes 1: Comparison with observations and evaluation of a layered approach. *Atmospheric Environment* **2000**, *34*, 3939–3950. doi:10.1016/S1352-2310(00)00156-4.
4. Workbook for plume visual impact screening and analysis (revised). Technical report, United States Environmental Protection Agency (EPA), 1992.
5. Paoli, R.; Cariolle, D.; Sausen, R. Review of effective emissions modeling and computation. *Geoscientific Model Development* **2011**, *4*, 643–667. doi:10.5194/gmd-4-643-2011.
6. Fritz, T.M.; Eastham, S.D.; Speth, R.L.; Barrett, S.R. The role of plume-scale processes in long-term impacts of aircraft emissions. *Atmospheric Chemistry and Physics* **2020**, *20*, 5697–5727. doi:10.5194/acp-20-5697-2020.
7. Brasseur, G.; Cox, R.; Hauglustaine, D.; Isaksen, I.; Lelieveld, J.; Lister, D.; Sausen, R.; Schumann, U.; Wahner, A.; Wiesen, P. European scientific assessment of the atmospheric effects of aircraft emissions. *Atmospheric Environment* **1998**, *32*, 2329–2418. doi: 10.1016/S1352-2310(97)00486-X.
8. Schlager, H.; Konopka, P.; Schulte, P.; Schumann, U.; Ziereis, H.; Arnold, F.; Klemm, M.; Hagen, D.E.; Whitefield, P.D.; Ovarlez, J. In situ observations of air traffic emission signatures in the North Atlantic flight corridor. *Journal of Geophysical Research* **1997**, *102*, 10739–10750. doi:10.1029/96JD03748.
9. Gössling, S.; Humpe, A. The global scale, distribution and growth of aviation: Implications for climate change. *Global Environmental Change* **2020**, *65*. doi: 10.1016/j.gloenvcha.2020.102194.
10. Anderson, J.D. *Aircraft perfomance and design*; Vol. 358, 1999; pp. 1–41.
11. Oates, G.C. *Aircraft Propulsion Systems Technology and Design*; 1989. doi:10.2514/4.861499.
12. Richter, H. *Advanced control of turbofan engines*; 2012; pp. 1–266.
13. Holladay, J.; Abdullah, Z.; Heyne, J. Sustainable Aviation Fuel: Review of Technical Pathways. Technical report, U.S Department of Energy, 2020.
14. Penner, J.; Lister, D.; Griggs, D.; Dokken, D.; McFarland, M., Aviation and the Global Atmosphere; Cambridge University Press, 1999; chapter 2.
15. Döpelheuer, A. Aircraft emission parameter modelling. *Air & Space Europe* **2000**, *2*, 34–37. doi:10.1016/S1290-0958(00)80060-X.
16. Dopelheuer, A.; Lecht, M. Influence of engine performance on emission characteristics. *RTO-Symposium of AVT on Gas Turbine Engine Combustion, Emissions and Alternative Fuels* **1998**.
17. Deidewig, F.; Dopelheuer, A.; Lecht, M. Methods to Assess Aircraft Engine Emissions in Flight. Technical report, 1996.
18. Gettelman, A.; Chen, C. The climate impact of aviation aerosols. *Geophysical Research Letters* **2013**, *40*, 2785–2789. doi:10.1002/grl.50520.
19. Aircraft fuels and their effect upon engine emissions. *Air & Space Europe* **2001**, *3*, 101–103. doi:10.1016/s1290-0958(01)90026-7.
20. Bockhorn, H., Soot Formation in Combustion; Springer, Berlin, Heidelberg, 1994.
21. Wayson, R.L.; Fleming, G.G.; Iovinelli, R.; Wayson, R.L.; Fleming, G.G.; Iovinelli, R.; Wayson, R.L.; Fleming, G.G. Methodology to Estimate Particulate Matter Emissions from Certified

Commercial Aircraft Engines Methodology to Estimate Particulate Matter Emissions from Certified Commercial Aircraft Engines **2012**. *2247*. doi:10.3155/1047-3289.59.1.91.

22. Schumann, U.; Arnold, F.; Busen, R.; Curtius, J.; Ka, B.; Kiendler, A.; Petzold, A.; Wohlfrom, K. Influence of fuel sulfur on the composition of aircraft exhaust plumes : The experiments SULFUR 1 – 7 **2002**. *107*.
23. Nuic, A.; Poles, D.; Mouillet, V. BADA: An advanced aircraft performance model for present and future ATM systems. *International Journal of Adaptive Control and Signal Processing* **2010**, *24*, 850–866. doi:10.1002/acs.1176.
24. Piano-X Aircraft Emissions and Performance User's Guide. Technical report, Lissys Ltd, 2008.
25. Aviation Environment Design Tool (AEDT) 2a: Technical Manual, Version 3c. Technical report, Federal Aviation Administration (FAA), 2020.
26. Sun, J.; Hoekstra, J.M.; Ellerbroek, J. OpenAP: An Open-Source Aircraft Performance Model for Air Transportation Studies and Simulations. *Aerospace* **2020**, *7*, 104. doi: 10.3390/aerospace7080104.
27. International Civil Aviation Organization (ICAO) Committee on Aviation Environmental Protection (CAEP). *ICAO Aircraft Engine Emissions Databank*, 28 ed.; 2021.
28. International Civil Aviation Organization (ICAO). Annex 16 to the Convention on International Civil Aviation–Volume I–Aircraft Noise. *Icao* **2008**, *552*.
29. SAE Aerospace. *Procedure for the Calculation of Aircraft Emissions*, 2009. doi: https://doi.org/10.4271/AIR5715.
30. Wasiuk, D.K. Modelling aircraft emissions and their impact on atmospheric composition and ozone. PhD thesis, University of Bristol, 2014.
31. Wasiuk, D.K.; Khan, A.H.; Shallcross, D.E.; Lowenberg, M.H. A Commercial Aircraft Fuel Burn and Emissions **2016**. *7*, 78. doi:10.3390/atmos7060078.
32. Mark Z. Jacobson. *Fundamentals of Atmospheric Modeling*, 2nd ed.; Cambridge University Press, 2005; [arXiv:1011.1669v3].
33. Petry, H.; Hendricks, J.; Möllhoff, M.; Lippert, E.; Meier, A.; Ebel, A.; Sausen, R. Chemical conversion of subsonic aircraft emissions in the dispersing plume: Calculation of effective emission indices. *Journal of Geophysical Research: Atmospheres* **1998**, *103*, 5759–5772. doi: 10.1029/97JD03749.
34. Cariolle, D.; Caro, D.; Paoli, R.; Hauglustaine, D.A.; Cuénot, B.; Cozic, A.; Paugam, R. Parameterization of plume chemistry into large-scale atmospheric models: Application to aircraft NOx emissions. *Journal of Geophysical Research Atmospheres* **2009**, *114*, 1–21. doi: 10.1029/2009JD011873.
35. Danilin, M.Y.; Ebel, A.; Elbern, H.; Petry, H. Evolution of the concentrations of trace species in an aircraft plume: trajectory study. *Journal of Geophysical Research* **1994**, *99*. doi: 10.1029/94jd01820.
36. Paoli, R.; Shariff, K. Contrail Modeling and Simulation. *Annual Review of Fluid Mechanics* **2016**, *48*, 393–427. doi:10.1146/annurev-fluid-010814-013619.
37. Gerz, T.; Dürbeck, T.; Konopka, P. Transport and effective diffusion of aircraft emissions. *Journal of Geophysical Research Atmospheres* **1998**, *103*, 25905–25913. doi:10.1029/98JD02282.
38. Crow, S.C. Stability Theory for a Pair of Trailing Vortices. *AIAA Journal* **1970**, *8*, 2172–2179. doi:10.2514/3.6083.
39. Unterstrasser, S.; Paoli, R.; Sölch, I.; Kühnlein, C.; Gerz, T. Dimension of aircraft exhaust plumes at cruise conditions: Effect of wake vortices. *Atmospheric Chemistry and Physics* **2014**, *14*, 2713–2733. doi:10.5194/acp-14-2713-2014.
40. Schumann, U.; Konopka, P.; Baumann, R.; Busen, R.; Gerz, T.; Schlager, H.; Schulte, P.; Volkert, H. Estimate of diffusion parameters of aircraft exhaust plumes near the tropopause from nitric oxide and turbulence measurements. *Journal of Geophysical Research* **1995**, *100*, 14147–14162.
41. Schumann, U.; Schlager, H.; Arnold, F.; Baumann, R.; Haschberger, P.; Klemm, O. Dilution of aircraft exhaust plumes at cruise altitudes. *Atmospheric Environment* **1998**, *32*, 3097–3103. doi: 10.1016/S1352-2310(97)00455-X.
42. Konopka, P. Analytical Gaussian Solutions for Anisotropie Diffusion in a Linear Shear Flow. *Journal of Non-Equilibrium Thermodynamics* **1995**, *20*. doi:10.1515/jnet.1995.20.1.78.
43. Vohralik, P.F.; Randeniya, L.K.; Plumb, I.C.; Baughcum, S.L. Effect of plume processes on aircraft impact. *Journal of Geophysical Research Atmospheres* **2008**, *113*, 1–21. doi: 10.1029/2007JD008982.

44. Dürbeck, T.; Gerz, T. Large-eddy simulation of aircraft exhaust plumes in the free atmosphere: Effective diffusivities and cross-sections. *Geophysical Research Letters* **1995**, *22*, 3203–3206. doi:10.1029/95GL03021.
45. Meijer, E. Modelling the impact of subsonic aviation on the composition of the atmosphere. PhD thesis, Applied Physics, 2001. doi:10.6100/IR550468.
46. Melo, O.T.; Lusis, M.A.; Stevens, R.D.S. *Atmospheric Environment* **1978**, *12*, 1231–1234.
47. Dürbeck, T.; Gerz, T. Dispersion of aircraft exhausts in the free atmosphere. *Journal of Geophysical Research Atmospheres* **1996**, *101*, 26007–26015. doi:10.1029/96jd02217.
48. Fritz, T.M. personal communication.
49. Lewellen, D.C.; Lewellen, W.S.; Poole, L.R.; DeCoursey, R.J.; Hansen, G.M.; Hostetler, C.A.; Kent, G.S. Large-eddy simulations and lidar measurements of vortex-pair breakup in aircraft wakes. *AIAA Journal* **1998**, *36*, 1439–1445. doi:10.2514/2.535.
50. Paoli, R. Large-eddy simulation of a turbulent jet and a vortex sheet interaction : particle formation and evolution in the near field of an aircraft wake **2008**. doi: 10.1127/0941-2948/2008/0278.
51. Secretariat General. *Annex 11 Environment*; Number July, 2016; p. 18.
52. Zhang, W.; Kamgarpour, M.; Sun, D.; Tomlin, C.J. A hierarchical flight planning framework for air traffic management. *Proceedings of the IEEE* **2012**, *100*, 179–194. doi: 10.1109/JPROC.2011.2161243.
53. Baumgartner, M.; Cook, A.; Dennis, N.; Houtte, B.V.; Majumdar, A.; Pilon, N.; Tanner, G.; Williams, V. European Air Traffic Management: Principles, Practice and Research **2007**. p. 255.
54. Mitchell, J.S.; Polishchuk, V.; Krozel, J. Airspace throughput analysis considering stochastic weather. *Collection of Technical Papers - AIAA Guidance, Navigation, and Control Conference 2006* **2006**, *8*, 5070–5088. doi:10.2514/6.2006-6770.
55. Krozel, J.; Mitchell, J.S.; Polishchuk, V.; Prete, J. Capacity estimation for airspaces with convective weather constraints. *Collection of Technical Papers - AIAA Guidance, Navigation, and Control Conference 2007* **2007**, *2*, 1518–1532. doi:10.2514/6.2007-6451.
56. Federal Aviation Administration. FAQ: Weather Delay, 2021.
57. International Civil Aviation Authority. *Doc 4444 - Air Traffic Management - Procedures for Air Navigation Services*, 16 ed.; 2016.
58. The Flow Management Problem in Air Traffic Control. In *Flow control of congested networks*; Springer-Verlag Berlin Heidelberg, 1987; Vol. 38, pp. 269–288.
59. Bilimoria, K.D.; Sridhar, B.; Chatterji, G.B. Effects of conflict resolution maneuvers and traffic density on free flight. *1996 Guidance, Navigation, and Control Conference and Exhibit* **1996**, pp. 1–12. doi:10.2514/6.1996-3767.
60. Federal Aviation Administration., Instrument Procedures Handbook (IPH); 2017; chapter 2. En Route Operations.
61. Soler, M.; Olivares, A.; Staffetti, E. Multiphase optimal control framework for commercial aircraft four-dimensional flight-planning problems. *Journal of Aircraft* **2015**, *52*, 274–286. doi: 10.2514/1.C032697.
62. Altus, S. Effective Flight Plans Can Help Airlines Economize. https://www.boeing.com/commercial/aeromagazine/articles/qtr_03_09/pdfs/AERO_Q309_article08.pdf.
63. Murrieta-Mendoza, A.; Botez, R. Lateral navigation optimization considering winds and temperatures for fixed altitude cruise using Dijsktra's algorithm. *ASME International Mechanical Engineering Congress and Exposition, Proceedings (IMECE)* **2014**, *1*, 1–9. doi: 10.1115/IMECE2014-37570.
64. Ng, H.K.; Sridhar, B.; Grabbe, S. A practical approach for optimizing aircraft trajectories in winds. 2012 IEEE/AIAA 31st Digital Avionics Systems Conference (DASC). IEEE, 2012.
65. Majumdar, A.; Ochieng, W.Y.; McAuley, G.; Lenzi, J.M.; Lepadatu, C. The factors affecting airspace capacity in Europe: A cross-sectional time-series analysis using simulated controller workload data. *Journal of Navigation* **2004**, *57*, 385–405. doi:10.1017/S0373463304002863.
66. Welch, J.D.; Andrews, J.W.; Martin, B.D.; Sridhar, B. Macroscopic workload model for estimating en route sector capacity. *Proceedings of the 7th USA/Europe Air Traffic Management Research and Development Seminar, ATM 2007* **2007**, pp. 94–103.
67. Gardi, A.; Sabatini, R.; Ramasamy, S. Multi-objective optimisation of aircraft flight trajectories in the ATM and avionics context. *Progress in Aerospace Sciences* **2016**, *83*, 1–36. doi:10.1016/j.paerosci.2015.11.006.

68. Olsen, S.C.; Wuebbles, D.J.; Owen, B. Comparison of global 3-D aviation emissions datasets. *Atmospheric Chemistry and Physics* **2013**, *13*, 429–441. doi:10.5194/acp-13-429-2013.
69. North Atlantic Tracks - Flight Plan database. https://flightplandatabase.com/nav/NATS.
70. Kärcher, B.; Meilinger, S.K. Perturbation of the aerosol layer by aviation-produced aerosols: A parametrization of plume processes. *Geophysical Research Letters* **1998**, *25*, 4465–4468. doi:10.1029/1998GL900183.
71. Brunton, J. North Atlantic Skies – The gateway to Europe. https://nats.aero/blog/2014/06/north-atlantic-skies-gateway-europe/, 2014.
72. Air transport, passengers carried. https://data.worldbank.org/indicator/IS.AIR.PSGR.
73. Schumann, U.; Schlager, H.; Arnold, F.; Ovarlez, J.; Kelder, H.; Hov.; Hayman, G.; Isaksen, I.S.; Staehelin, J.; Whitefield, P.D. Pollution from aircraft emissions in the North Atlantic flight corridor: Overview on the POLINAT projects. *Journal of Geophysical Research Atmospheres* **2000**, *105*, 3605–3631. doi:10.1029/1999JD900941.
74. Thompson, A.M.; Singh, H.B.; Schlager, H. Introduction to special section: Subsonic assessment ozone and nitrogen oxide experiment (SONEX) and Pollution from aircraft emissions in the north atlantic flight corridor (POLINAT 2). *Journal of Geophysical Research: Atmospheres* **2000**, *105*, 3595–3603. doi:10.1029/2000JD900012.
75. on Climate Change, I.P., Anthropogenic and Natural Radiative Forcing. In *Climate Change 2013 – The Physical Science Basis: Working Group I Contribution to the Fifth Assessment Report of the Intergovernmental Panel on Climate Change*; Cambridge University Press, 2014; p. 659–740. doi:10.1017/CBO9781107415324.018.
76. Gettelman, A.; Pan, L.L.; Randel, W.J.; Hoor, P.; Birner, T.; Hegglin, M.I. the Extratropical Upper Troposphere and Lower Stratosphere. *Reviews of Geophysics* **2011**, *49*, 1–31. doi:10.1029/2011RG000355.1.INTRODUCTION.
77. Schumann, U. The impact of nitrogen oxides emissions from aircraft upon the atmosphere at flight altitudes - Results from the aeronox project. *Atmospheric Environment* **1997**, *31*, 1723–1733. doi:10.1016/S1352-2310(96)00326-3.
78. Johnson, C.; Henshaw, J.; Mclnnest, G. Impact of aircraft and surface emissions of nitrogen oxides on tropospheric ozone and global warming **1992**. *355*, 69–71.
79. Lee, D.; Pitari, G.; Grewe, V.; Gierens, K.; Penner, J.; Petzold, A.; Prather, M.; Schumann, U.; Bais, A.; Berntsen, T. Transport impacts on atmosphere and climate: Aviation. *Atmospheric Environment* **2010**, *44*, 4678–4734. doi:10.1016/j.atmosenv.2009.06.005.
80. Grewe, V.; Dameris, M.; Fichter, C.; Sausen, R. Impact of aircraft NOx emissions. Part 1: Interactively coupled climate-chemistry simulations and sensitivities to climate-chemistry feedback, lightning and model resolution. *Meteorologische Zeitschrift* **2002**, *11*, 177–186. doi:10.1127/0941-2948/2002/0011-0177.
81. Forster, C. The residence times of aircraft emissions in the stratosphere using a mean emission inventory and emissions along actual flight tracks. *Journal of Geophysical Research* **2003**, *108*, 8524. doi:10.1029/2002JD002515.
82. Fuglestvedt, J.S.; Berntsen, T.K.; Godal, O.; Sausen, R.; Shine, K.P.; Skodvin, T. Metrics of climate change: Assessing radiative forcing and emission indices. *Climatic Change* **2003**, *58*, 267–331. doi:10.1023/A:1023905326842.
83. Schneider, S.H. The Greenhouse Effect: Science and Policy. *Science* **1989**, *243*, 771–781. doi:10.1126/science.243.4892.771.
84. Archer, D.; Brovkin, V. The millennial atmospheric lifetime of anthropogenic CO2 **2008**. *90*, 283–297. doi:10.1007/s10584-008-9413-1.
85. Burkhardt, U.; Kärcher, B. Global radiative forcing from contrail cirrus. *Nature Climate Change* **2011**, *1*, 54–58. doi:10.1038/nclimate1068.
86. Schumann, U. Formation, properties and climatic effects of contrails. *Comptes Rendus Physique* **2005**, *6*, 549–565. doi:10.1016/j.crhy.2005.05.002.
87. Appleman, H. The Formation of Exhaust Condensation Trails by Jet Aircraft. *Bulletin of the American Meteorological Society* **1953**, *34*, 14–20. doi:10.1175/1520-0477-34.1.14.
88. Schumann, U. Contrails - a prototype of cirrus cloud studies since 80 years. *Meteorol. Zeitschrift* **1997**, *6*, 304–305.
89. Schumann, U. On conditions for contrail formation from aircraft exhausts. *Meteorologische Zeitschrift* **1996**, *5*, 4–23. doi:10.1127/metz/5/1996/4.
90. Tait, K. Assessing the effectiveness of contrail diversion schemes in mitigating aviation-induced climate change. Master's thesis, 2020.

91. Spichtinger, P.; Leschner, M. Tellus B : Chemical and Physical Meteorology Horizontal scales of ice-supersaturated regions **2016**. *0889*.
92. Vertical spatial scales of ice supersaturation and probability of ice supersaturated layers in low resolution profiles of relative humidity. *DLR Deutsches Zentrum fur Luft- und Raumfahrt e.V. - Forschungsberichte* **2010**, pp. 239–243.
93. Schumann, U.; Graf, K.; Mannstein, H. Potential to reduce the climate impact of aviation by flight level changes. 3rd AIAA Atmospheric Space Environments Conference. American Institute of Aeronautics and Astronautics, 2011. doi:10.2514/6.2011-3376.
94. Schumann, U.; Heymsfield, A.J. On the Life Cycle of Individual Contrails and Contrail Cirrus. *Meteorological Monographs* **2017**, *58*, 3.1–3.24. doi: 10.1175/AMSMONOGRAPHS-D-16-0005.1.
95. Newinger, C.; Burkhardt, U. Sensitivity of contrail cirrus radiative forcing to air traffic scheduling. *Journal of Geophysical Research Atmospheres* **2012**, *117*, 1–12. doi: 10.1029/2011JD016736.
96. Kärcher, B.; Burkhardt, U.; Bier, A.; Bock, L.; Ford, I.J. The microphysical pathway to contrail formation. *Journal of Geophysical Research: Atmospheres* **2015**, *120*, 7893–7927. doi: 10.1002/2015JD023491.
97. Stevenson, D.S.; Doherty, R.M.; Sanderson, M.G.; Collins, W.J.; Johnson, C.E.; Derwent, R.G. Radiative forcing from aircraft NOx emissions: Mechanisms and seasonal dependence. *Journal of Geophysical Research D: Atmospheres* **2004**, *109*. doi:10.1029/2004JD004759.
98. Wild, O.; Prather, M.J.; Akimoto, H. Indirect from long-term global radiative emissions cooling. *October* **2001**, *28*, 1719–1722.
99. Myhre, G.; Shine, K.; Rädel, G.; Gauss, M.; Isaksen, I.; Tang, Q.; Prather, M.; Williams, J.; van Velthoven, P.; Dessens, O.; Koffi, B.; Szopa, S.; Hoor, P.; Grewe, V.; Borken-Kleefeld, J.; Berntsen, T.; Fuglestvedt, J. Radiative forcing due to changes in ozone and methane caused by the transport sector. *Atmospheric Environment* **2011**, *45*, 387–394. doi: 10.1016/j.atmosenv.2010.10.001.
100. Holmes, C.D.; Tang, Q.; Prather, M.J. Uncertainties in climate assessment for the case of aviation NO. *Proceedings of the National Academy of Sciences* **2011**, *108*, 10997–11002. doi: 10.1073/pnas.1101458108.
101. Myhre, G.; Nilsen, J.S.; Gulstad, L.; Shine, K.P.; Rognerud, B.; Isaksen, I.S. Radiative forcing due to stratospheric water vapour from CH4 oxidation. *Geophysical Research Letters* **2007**, *34*, 1–5. doi:10.1029/2006GL027472.
102. Bond, T.C.; Doherty, S.J.; Fahey, D.W.; Forster, P.M.; Berntsen, T.; DeAngelo, B.J.; Flanner, M.G.; Ghan, S.; Kärcher, B.; Koch, D.; Kinne, S.; Kondo, Y.; Quinn, P.K.; Sarofim, M.C.; Schultz, M.G.; Schulz, M.; Venkataraman, C.; Zhang, H.; Zhang, S.; Bellouin, N.; Guttikunda, S.K.; Hopke, P.K.; Jacobson, M.Z.; Kaiser, J.W.; Klimont, Z.; Lohmann, U.; Schwarz, J.P.; Shindell, D.; Storelvmo, T.; Warren, S.G.; Zender, C.S. Bounding the role of black carbon in the climate system: A scientific assessment. *Journal of Geophysical Research: Atmospheres* **2013**, *118*, 5380–5552. doi:10.1002/jgrd.50171.
103. Brown, R.C.; Anderson, M.R.; Miake-Lye, R.C.; Kolb, C.E.; Sorokin, A.A.; Buriko, Y.Y. Aircraft exhaust sulfur emissions. *Geophysical Research Letters* **1996**, *23*, 3603–3606. doi: https://doi.org/10.1029/96GL03339.
104. Penner, J.E.; Zhou, C.; Garnier, A.; Mitchell, D.L. Anthropogenic Aerosol Indirect Effects in Cirrus Clouds. *Journal of Geophysical Research: Atmospheres* **2018**, *123*, 11,652–11,677. doi: 10.1029/2018JD029204.
105. Meijer, E.W.; Van Velthoven, P.F.; Wauben, W.M.; Beck, J.P.; Velders, G.J. The effects of the conversion of nitrogen oxides in aircraft exhaust plumes in global models. *Geophysical Research Letters* **1997**, *24*, 3013–3016. doi:10.1029/97GL53156.


**Author Contributions:** For research articles with several authors, a short paragraph specifying their individual contributions must be provided. The following statements should be used "Conceptualization, X.X. and Y.Y.; methodology, X.X.; software, X.X.; validation, X.X., Y.Y. and Z.Z.; formal analysis, X.X.; investigation, X.X.; resources, X.X.; data curation, X.X.; writing—original draft preparation, X.X.; writing—review and editing, X.X.; visualization, X.X.; supervision, X.X.; project administration, X.X.; funding acquisition, Y.Y. All authors have read and agreed to the published version of the manuscript.", please turn to the CRediT taxonomy for the term explanation. Authorship must be limited to those who have contributed substantially to the work reported.

**Funding:** Please add: "This research received no external funding" or "This research was funded by NAME OF FUNDER grant number XXX." and and "The APC was funded by XXX". Check carefully that the details given are accurate and use the standard spelling of funding agency names at https://search.crossref.org/funding, any errors may affect your future funding.

**Institutional Review Board Statement:** In this section, please add the Institutional Review Board Statement and approval number for studies involving humans or animals. Please note that the Editorial Office might ask you for further information. Please add "The study was conducted according to the guidelines of the Declaration of Helsinki, and approved by the Institutional Review Board (or Ethics Committee) of NAME OF INSTITUTE (protocol code XXX and date of approval)." OR "Ethical review and approval were waived for this study, due to REASON (please provide a detailed justification)." OR "Not applicable" for studies not involving humans or animals. You might also choose to exclude this statement if the study did not involve humans or animals.

**Informed Consent Statement:** Any research article describing a study involving humans should contain this statement. Please add "Informed consent was obtained from all subjects involved in the study." OR "Patient consent was waived due to REASON (please provide a detailed justification)." OR "Not applicable" for studies not involving humans. You might also choose to exclude this statement if the study did not involve humans.
Written informed consent for publication must be obtained from participating patients who can be identified (including by the patients themselves). Please state "Written informed consent has been obtained from the patient(s) to publish this paper" if applicable.

**Data Availability Statement:** In this section, please provide details regarding where data supporting reported results can be found, including links to publicly archived datasets analyzed or generated during the study. Please refer to suggested Data Availability Statements in section "MDPI Research Data Policies" at https://www.mdpi.com/ethics. You might choose to exclude this statement if the study did not report any data.

**Acknowledgments:** Thibaud M. Fritz (MIT), Stephen Roome,

**Conflicts of Interest:** Declare conflicts of interest or state "The authors declare no conflict of interest." Authors must identify and declare any personal circumstances or interest that may be perceived as inappropriately influencing the representation or interpretation of reported research results. Any role of the funders in the design of the study; in the collection, analyses or interpretation of data; in the writing of the manuscript, or in the decision to publish the results must be declared in this section. If there is no role, please state "The funders had no role in the design of the study; in the collection, analyses, or interpretation of data; in the writing of the manuscript, or in the decision to publish the results".

**Sample Availability:** Samples of the compounds ... are available from the authors.

## Abbreviations

The following abbreviations are used in this manuscript:

| | |
|---|---|
| MDPI | Multidisciplinary Digital Publishing Institute |
| DOAJ | Directory of open access journals |
| TLA | Three letter acronym |
| LD | Linear dichroism |

## Appendix A

### *Appendix A.1*

The appendix is an optional section that can contain details and data supplemental to the main text—for example, explanations of experimental details that would disrupt the flow of the main text but nonetheless remain crucial to understanding and reproducing the research shown; figures of replicates for experiments of which representative data are shown in the main text can be added here if brief, or as Supplementary Data. Mathematical proofs of results not central to the paper can be added as an appendix.

**Table A1.** This is a table caption. Tables should be placed in the main text near to the first time they are cited.

| Title 1 | Title 2 | Title 3 |
|---|---|---|
| Entry 1 | Data | Data |
| Entry 2 | Data | Data |

All appendix sections must be cited in the main text. In the appendices, Figures, Tables, etc. should be labeled, starting with "A"—e.g., Figure A1, Figure A2, etc.